2015

Characterization of Directionally Solidified Gray Iron

Elis Annexy Rivera-Martinez
University of Alabama at Birmingham

CHARACTERIZATION OF DIRECTIONALLY SOLIDIFIED GRAY IRON

by

ELIS A. RIVERA-MARTINEZ

AMBER GENAU, COMMITTEE CHAIR
CHARLES MONROE
ROBIN FOLEY
JOHN GRIFFIN

A MASTER THESIS

Submitted to the graduate faculty of The University of Alabama at Birmingham,
in partial fulfillment of the requirements for the degree of
Master of Science

BIRMINGHAM, ALABAMA

April 2015

CHARACTERIZATION OF DIRECTIONALLY SOLIDIFIED GRAY IRON

ELIS A RIVERA-MARTINEZ

MATERIALS SCIENCE AND ENGINEERING

ABSTRACT

Even with decades of study, the complex development of solidification microstructures in cast iron is incompletely understood. Because Fe-C eutectic can produce different morphologies, and even different phases, depending on growth velocities and composition, understanding the conditions under which each forms are important. Directional solidification was used to observe the behavior of gray cast iron under carefully controlled solidification conditions. Specifically, alloys with industrially relevant amounts of silicon and manganese were studied, using a Bridgman furnace to investigate the effects of alloying additions and solidification velocity on graphite spacing and growth temperature of gray iron. An experimental technique for measuring the solid/liquid interface temperature was developed, producing precise temperature curves of the samples during the directional solidification. Average and minimum spacing for five compositions, containing varied amounts of Si and Mn, and velocities from 0.5 to 10 μm/s are reported. A critical velocity of around 1 μm/s was observed, above which the graphite structure loses directionality and austenite dendrites appear. A recently developed automated MATLAB algorithm was used for quickly and objectively measuring graphite spacing. The automated results compare favorably with traditional manual measurements and will allow for more robust measurement of eutectic spacing in a variety of systems where the spacing is highly irregular. Lastly, graphite spacing in gray

iron was measured, showing a dependence on both velocity and composition. Adding silicon and manganese to the gray iron showed a decrease in spacing; while increasing the velocity seemed to affect directionality and reduce flake graphite thickness. Transverse section spacing and the carbon percentage versus distance of solidification analysis presented that graphite spacing and the carbon percentage varies with solidification distance.

Keywords: Gray Iron, Cast Iron, Eutectic, Directional Solidification, Graphite Spacing, Stereology

ACKNOWLEDGMENTS

To begin with, I would like to offer my honest appreciation and gratitude to my advisor, mentor and committee chairman, Dr. Amber Genau, for the continued patience, support, encouragement and knowledge that was bestowed upon me by her great efforts. Because of her positive attitude, ideas and direction on this project, as well as my future professional career, I had the opportunity to develop myself into a much better researcher, engineer and person than what I have ever imagined.

In addition, I would like to thank Dr. Charles Monroe, who I also owe my future professional career as an engineer. Thanks to his support, encouragement and insight, I was able to get the type of experience that would determine my future in the engineering world. My sincerest gratitude also goes to Dr. Robin Foley and Mr. John Griffin for the knowledge and aid that they have continuously given me through my graduate school career in UAB. Both of their efforts, patience and resourcefulness has always been appreciated and it serves me as inspiration to emulate such wonderful values as a professional and as a person.

Special thanks to: Dr. Barry Andrews for providing support since the beginning of my graduate school career and has always provided theoretical and technical support throughout my time in the solidifications laboratory. I would like to thank William Stonewall Monroe for his time, comments and patience in creating and modifying the algorithm used in this project for the analysis of my samples. Additionally, I would like to give my gratitude to undergraduate students Tyler Christiansen and Kelly Dillon for their aid in this project. Thanks to both of them because the project was able to move forward, especially those times where I was not present to continue it myself.

I definitely would like to thank also, my fellow graduate student labmates in the casting group, both past and present: Carlos Colina, Siddharta Biswas, Alex Noble, Nic Willis, Rhiannon Bragg, Chunlei Wang, Jun Ge, and William Warriner. I would have never been able to go through this adventure without any of you. Moreover, I would have never made it through this odyssey at all without two of the most important casting group members in my eyes: Subhojit Chakraborty and Maria Diana David. Both of them have always offered me great insight on academic, professional and personal matters that, if not because of their words and company, this document would, most definitely, not have been submitted at all. A very special thanks to Subhojit Chakraborty for aiding me into realizing the second part of what is to me, the most important lesson of my academic career: "You are not expected to know everything, but you are expected to learn everything". My most sincere gratitude also to the other graduate students from the MSE department from previous and current years: Alejandra Constante, Kristin Hardin, Sid Brahma, Carrie Schindler, and all others I forgot to mention who were in one way or another part of my graduate life at UAB.

Lastly, I want to thank, my parents, my siblings, and all my family and friends that are in Puerto Rico or the USA, for their support in my career and for aiding me in reaching my goal of getting a graduate degree, let it be by words of encouragement, by a friendly hug or by telling me that I should stop overthinking, as I usually do, and get my stuff together. Thanks all for the never ending support and inspiration.

Portions of this work were funded by Department of Energy award DE-EE005980, through Caterpillar Inc. and Questek Innovations LLC.

TABLE OF CONTENTS

Page

LIST OF TABLES

Table *Page*

LIST OF FIGURES

Figure *Page*

1. INTRODUCTION

Cast iron is a popular alloy containing primarily iron and carbon that is commonly used in the casting industry. Depending on solidification conditions and alloying additions, various types of iron can form that differ in structure and properties. These different irons can be divided into four main types: gray iron, white iron, ductile iron, and compacted graphite iron. Figure 1 shows the portion of the phase diagram for the Fe-C system relevant to cast iron. Technically, cast iron is any composition that passes through the eutectic reaction on the phase diagram (2.11-6.67 wt% C); however, the common range for cast iron is 2.1-4.0 wt% C. Silicon is ususally also added in the amount of 1-3 wt%. The phase diagram in Figure 1 actually shows two different phase diagrams: the equilibrium solid line shows the behavior of the stable phase graphite, while the dashed line shows the behavior of the metastable cementite phase. Gray iron forms from the eutectic solidification of austenite and graphite, while the eutectic solidification of austenite and cementite is known as white iron.

Gray iron is a type of cast iron with graphitic microstructure. The presence of graphite in the structure gives the fracture surface a gray color, from which it takes its name. Gray iron is a common engineering alloy that is preferred because of its low cost, good machinability, wear resistance, and excellent damping capacity. In addition, gray iron experiences less solidification shrinkage, and the silicon that it contains promotes good corrosion resistance and increases fluidity when casting [1]. The applications of this material are extensive; the most popular ones are used in internal combustion engine cylinder blocks, pump housings, electrical boxes and decorative castings.

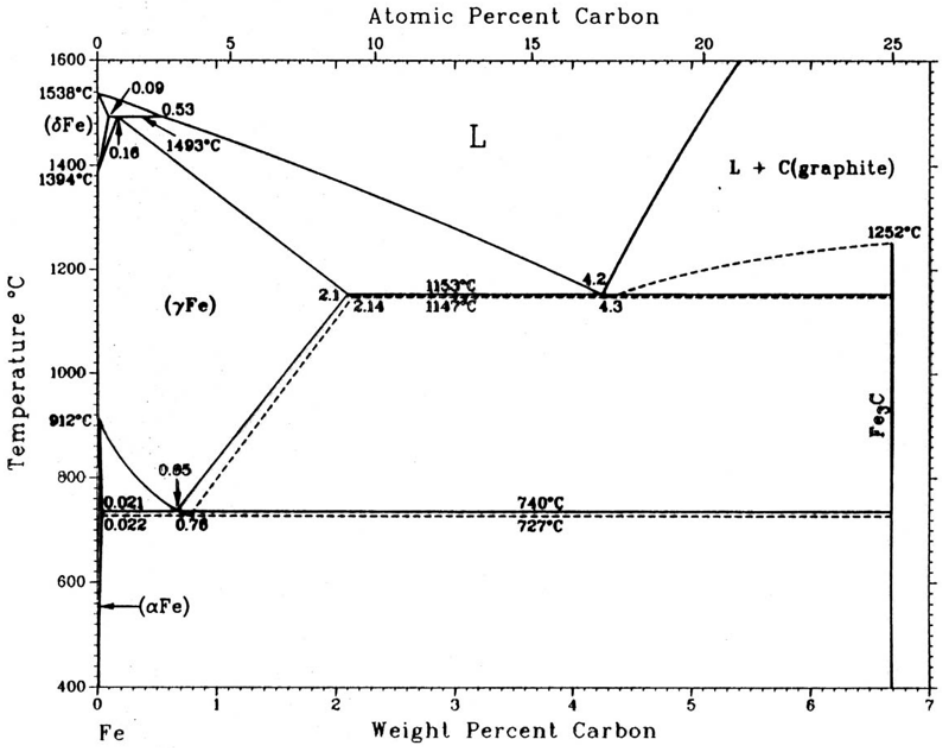

Figure 1: Phase diagram of iron and carbon showing both stable graphite structure (solid line), and metastable cementite structure (dashed) [2]

In cast iron, alloying elements are used to improve the structure and properties of the material. As mentioned, silicon is one of the most common alloying elements used for gray iron, the reason being that adding a small percentage of Si in the material improves its fluidity. Additionally, the phase diagram shows that there is a range in temperature in which graphite can be kept from appearing before the cementite structure starts to form. Silicon is also used to increase this temperature gap and give a larger range in which the melt will create graphite before it starts forming cementite. This will aid in converting more carbon into graphite than cementite. Figure 2 shows the effect of Si on the Fe-C phase diagram. As the figure shows, alloying elements can shift the eutectic temperature left and right as well as up and down. For this reason, a carbon equivalent equation is used. The equation predicts the necessary amount of carbon to obtain hypoeutectic,

eutectic or hypereutectic iron as a function of particular alloying elements. The equation for the carbon equivalent is shown in Equation 1 [3].

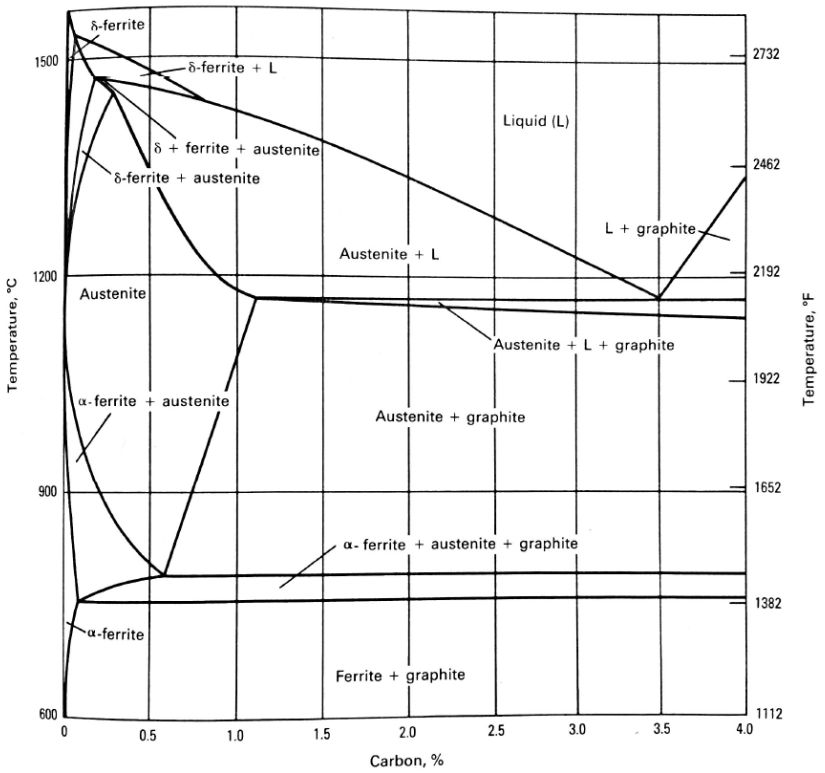

Figure 2: Effect of 2.5% silicon on phase diagram between graphite and cementite [4]

Equation 1: $$\boldsymbol{CE = \%C + 0.33(\%Si) + 0.33(\%P) - 0.027(\%Mn) + 0.4(\%S)}$$

White iron is the type of iron alloy that has austenite plus cementite in its structure, and forms at the faster cooling rates. In white cast iron, the metastable phase cementite, Fe_3C, precipitates out of the melt instead of graphite. It is very difficult to cool thick castings fast enough to solidify the melt as white iron all the way through. Nonetheless, rapid cooling can be used to solidify a shell of white cast iron, with the remainder cooling slowly forming gray iron.

Another difference between the two types of eutectic cast iron is that white iron forms a regular eutectic while gray iron forms an irregular eutectic, which grows differently due to the behavior at the solid/liquid interface. White iron is austenite with cementite, both of which grow with nonfaceted interfaces. In gray iron, the austenite phase remains nonfaceted while the graphite grows with a faceted interface. Faceting occurs in phases where the surface energy is highly anisotropic. The system, as it grows, tries to minimize the high surface energy and thus grows only in preferred crystallographic directions. Faceted interfaces have solid/liquid interfaces that grow atomically flat (atoms from the liquid accommodate only at certain sites). Because of this the atoms need time to be able to attach in the desired direction. The growth of faceted interfaces tends to be much slower than nonfaceted ones since the attachment kinetics are much slower [5]. The nonfaceted interface has no prefered crystallographic orientations so atoms will attach themselves to any available site. Nonfaceted interfaces are microscopically smooth but atomically rough. Figure 3 shows an image of how the faceted and nonfaceted interfaces look both atomically and microscopically.

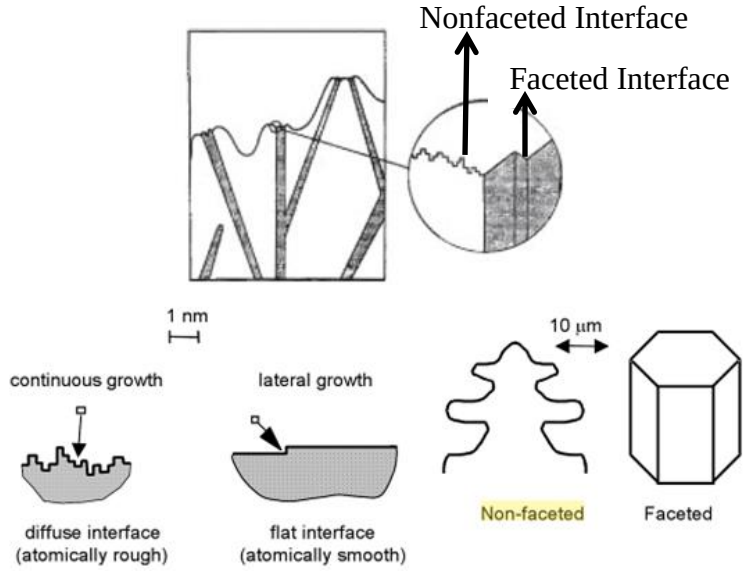

Figure 3: Faceted and non-faceted interface of an irregular eutectic gray iron (top). Atomic and microscopic designs of faceted and non-faceted interface (bottom)[6]

Since either graphite or cementite can form during cooling of cast iron, there is a competitive growth between white and gray iron. The outcome can be determined by either velocity or temperature. The basic rule of competitive growth is that during equiaxed solidification, when temperature is constant, the structure with the highest growth velocity will appear. During directional solidification, when velocity is fixed, then the structure with the highest growth temperature will be present. Figure 4 shows a plot from the work of H. Jones [7], showing that gray iron (EU1) is the preferred structure at low velocities. It is also seen that at moderate velocities austenite dendrites (AU) surrounded by gray eutectic are present and at high velocities white eutectic iron (EU2) is present. As an irregular eutectic, gray iron's growth temperature is sensitive to velocity; as the velocity increases, the interface temperature decreases significantly. The growth temperature of the regular eutectic, white iron, is relatively unaffected by velocity due to the fast attachment kinetics. This means that the transition temperature from white iron ($\gamma + Fe_3C$) to gray iron (γ + flake graphite) varies with solidification velocity.

For moderate velocities, austenite dendrites are present because the system has exceeded the critical velocity. Critical velocity is the velocity at which a solid/liquid interface becomes unstable and protubations begin to grow. This concept is explained by constitutional supercooling, which occurs due to compositional changes and results in the liquid falling below the freezing temperature ahead of the solid/liquid interface. When solidifying a molten metal, the interface is often unstable due to the fact that it is below the point which it usually starts solidifying and the velocity of the solid/liquid interface must be small (or the thermal gradient very high) in order to avoid growth of protubations

(i.e. dendrites). If the velocity can be maintained below the critical velocity, then the interface will grow in a planar manner and dendrites can be avoided.

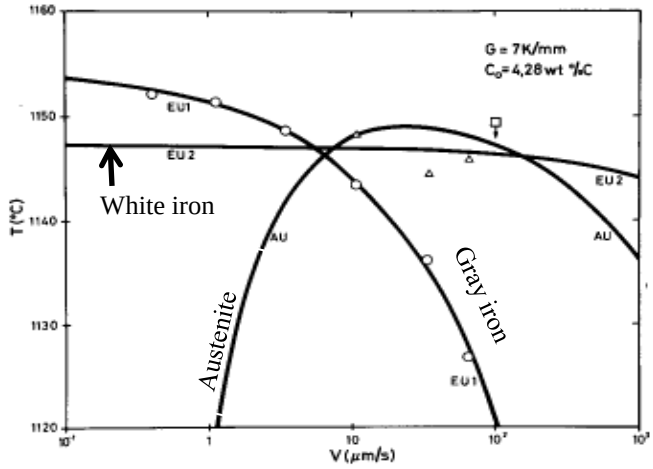

Figure 4: Plot of growth temperature as function for Fe-C[7]

Understanding and being able to predict the solidification behavior of cast iron is important because the type of graphite or cementite formation in cast iron is closely related to mechanical and other properties. The directionality, length and spacing of the phases in the cast iron will ultimately affect mechanical properties such as fatigue in the material that could mean an advantage for engineering applications.

The goal of this work was to measure the eutectic growth temperature and graphite spacing in gray iron using directional solidification. It will provide benchmark data that will be used to validate a new quantitative model for predicting the behavior in cast iron with ternary or quaternary alloying elements. This project extends the work of P. Magnin and W. Kurz [8] by considering specific alloy compositions that are particularly relevant to modern foundry industries. Directional solidification in a Bridgman furnace was used to obtain the experimental results.

1.1. Background

Directional solidification is a well-known process for investigating the behavior of materials under well-controlled solidification conditions. Directional solidification on gray iron samples started in the early 1960s [9] and has shown changes in constitution, morphology and spacing with the variation of growth velocity and composition. Since then, more studies by various researchers have been published in an effort to comprehend the behavior of the complex cast iron. Some of the most significant research about directionally solidified gray and white iron was done by P. Magnin and W. Kurz [8]. The paper discusses the well-known equation of lamellar spacing given by K.A Jackson and J.D Hunt in 1966 [10]. The relationship shows that lamellar spacing (λ) equals a constant (K) divided by the square root of the growth velocity ($\lambda = K/\sqrt{V}$). This relationship was established for white cast iron which is a regular eutectic, but also holds true for irregular eutectics (gray iron) if the constant K is modified for the type of eutectic. In Magnin and Kurz's work, they describe the competitive growth of stable and metastable Fe-C eutectic with small additions of Si, P, Cr, Mn, Ti, Al and S. The samples used by the researchers were slightly hypereutectic. Their results show that at low solidification rates, gray morphology is purely graphite flakes with no austenite dendrites present. They also found that sulfur content increases the spacing of gray eutectic, while other elements have no effect. For intermediate velocities of solidification (higher than 5 μm/s or 15 μm/s in the presence of sulfur), the spacing of the eutectic displays a higher value than the one predicted. Additional effects on structure, such as spacing increasing upon increasing velocity from 20 to 200 μm/s with the presence of manganese, can be explained by a progressive transition from a lamellar to more fiber-like eutectic [8].

Spacing and growth temperature information about gray iron is also discussed carefully in the ASM Handbook Volume 15: Casting of 2008[11]. In the handbook explains how the spacing within the graphite layers decreases away from the oxide until unconstrained spacing is reached. In addition, the different structures of cast iron with varying cooling rate and the shape of graphite are discussed. The work performed by theoretical relationship of Jackson and Hunt is discussed including the growth temperatures of gray iron. The cooling to shape ratio necessary to produce a planar interface during directional solidification is discussed.

It has been mentioned that the composition of the gray iron and the processing parameters have an effect on the structure, morphology and spacing of the material. From the research work of A. Kagawa and T. Okamoto[12], it is possible to see that zone melting, also named zone refining, was used to effectively determine the partition coefficient for silicon between the gray and white eutectic liquid and solid during solidification. They determined that the solid/liquid interface of both eutectics grows in a different manner during solidification. For both the partition and the size of solid/liquid interface, the stable gray eutectic showed higher values than the metastable white eutectic. Moreover, thermodynamic calculations for the equilibrium partition coefficient showed that these coefficients are highly dependent on silicon content, especially for austenite-graphite eutectic solidification. These theoretical evaluations were applicable to other alloying elements provided the thermodynamic data is available. Figure 5 shows the structure differences of both types of cast iron eutectics.

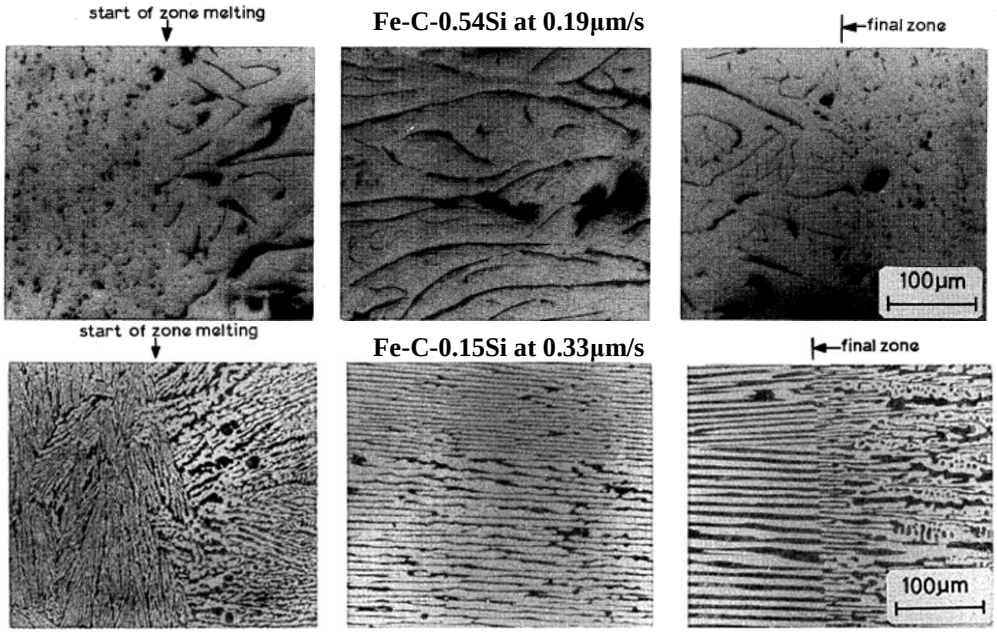

Figure 5: Gray iron eutectic (top) and white iron eutectic (bottom) directionally solidified [12]

New ideas of directionally solidified cast iron developed to improve the understanding of the material under other conditions. For example, alloys solidified at a low gravity environment will create unique and often desirable microstructures, due to the elimination of sedimentation and convection. Efforts to comprehend this phenomenon were done by J. C. Hendrix, P. A. Curreri and D. M. Stefanescu in 1984, when graphite cast iron was directionally solidified to study the behavior of the eutectic at low-g environments [13]. In the project, hypereutectic flake graphite cast iron with low and high phosphorous content and hypereutectic spheroidal graphite obtained through treatment with metallic cerium were compared. For both flake and spheroidal graphite, irons flotation of carbon occurred due to the high carbon equivalent when the sample solidifies at high gravity. In low gravity, no flotation occurred even with high carbon equivalents, which suggests the possibility of manufacturing iron-carbon alloys with high carbon content [13]. Manufacturing these materials could have a highly oriented structure

as a result of directional solidification if flake graphite structures are solidified. Furthermore, gravity can also have an effect on microstructural variation in directionally solidified eutectic iron carbon types of alloys. In the work done by Doru Stefanescu in 1986 showed a refinement of the interlamellar spacing of eutectic during low gravity processing of metastable Fe-C eutectic alloys[14]. Results for the stable eutectic (lamellar or spheroidal graphite) show a coarsening of the eutectic grain structure. Additionally, secondary dendrite arm spacing of the austenite dendrites increases at low-g and decreases with high-g. A low-g environment also helps in the removal of buoyancy-driven graphite phase segregation [14]. Through this work, it could be possible that low gravity environment will have an effect in the structure of the flake graphite in gray iron. This suggests that the graphite spacing itself will be affected, and in turn the gray iron's properties can also be manipulated.

The race between the growth of stable and metastable solidification in Fe-C base alloys is controlled by three constraints: the difference in growth temperatures between the white and gray eutectic, the undercooling essential for the nucleation of the cementite phase and lastly the growth undercooling of gray eutectic. All of the mentioned parameters can be related to the transition velocities ($V_{w\rightarrow g}$ & $V_{g\rightarrow w}$). Magnin and Kurz also concluded that the effect of alloying elements upon the transition velocities results from a complex combination of effects on the phase equilibria, and nucleation and growth kinetics. The literature written by the authors also indicate that the effect of element additions to Fe-C on the gray-to-white velocity is insufficient to determine $V_{g\rightarrow w}$ for a multicomponent alloy [15].

Studies to this point have shown that including additional alloys in the stable and metastable Fe-C eutectic has an effect on the preferred structure of growth. The efforts of P. Magnin and W. Kurz [8] explain the competitive growth stable and metastable Fe-C eutectic with small additions of Si, P, Cr, Mn, Ti, Al and S. Alloying elements can be classified into three types. Graphitizing elements (Si, Al, P and S) increase the velocity of transition from white to gray iron and from gray to white and stabilize graphite. Carburizing elements (Cr), are the second type and these lower the two transition velocities ($V_{w\rightarrow g}$ & $V_{g\rightarrow w}$) and make carbide more likely. The third type is the "hysteresis effect" (Mn, Ti), which increases $V_{g\rightarrow w}$ but lowers $V_{w\rightarrow g}$ and make the white structure more difficult to obtain. Growth temperatures and graphite spacing for gray eutectic as function of growth rate were also determined by the authors. Table 1 shows the graphite spacing for the materials used in their experiment. The thermocouple system that was employed for this experiment is shown in Figure 6 [16]. The image shows two type S thermocouples set up at a distance of 3 mm apart. The thermocouples are sheathed with alumina and inserted from the top of the crucible into the liquid zone of the sample. The sample was solidified and the thermocouples recorded the temperatures of the liquid zone. Once the solid/liquid interface passed through the thermocouples there was a notable difference in slope taken from the temperature curve that would represent the interface temperature. The growth rates shown in Table 2 clearly illustrate the effect of the additional alloys on the growth of gray iron.

Table 1: Spacing measurements given in micrometers for different solidification rates [8]

Alloy		Solidification Rate (μm/s)																			
		0.016	0.16	0.66	1	1.33	1.67	3.33	5	6.66	8.33	10	13.3	16.6	33.3	50	66.6	100	133	166	333	500
Fe-C	low G						16.8	10.9	9.1	9.4					8.5			6.0		7.9		
Fe-C	high G						16.4		10.0		11.8			8.7	6.9							
Fe-C-Si	0.1 pct			26.2	20.0		15.6	12.8	12.7	10.4				8.6		9.6	8.3					
Fe-C-Si	0.5 pct						14.9							8.2							6.7	
Fe-C-P	100 ppm							10.2		9.5		9.1	8.6	8.4	7.2		7.8	11.0				
Fe-C-P	0.1 pct						14.9		9.8			10.4		10.3						9.7		10.0
Fe-C-Cr	300 ppm						16.6	11.6	11.3			10.3		9.1	7.5					11.0		
Fe-C-Cr	0.5 pct	163	50.6																			
Fe-C-Mn	0.1 pct						15.9		10.0			7.9	7.9	9.4			9.9	9.7	7.8	7.9		
Fe-C-Mn	0.6 pct						15.3								6.9			7.4		8.3		
Fe-C-Ti	100 ppm						16.7					10.2		8.9	8.1	8.8	10.9	8.1				
Fe-C-Ti	0.2 pct						15.2	12.0		9.9				10.2	10.3		9.0	8.2	8.5	8.7		
Fe-C-Al	500 ppm						15.1		10.9	9.8				7.1		6.2		6.8	7.7	6.2		
Fe-C-Al	0.2 pct						15.8		9.3	8.3		7.2		6.9								
Fe-C-S	50 ppm						20.6							4.2		1.7		3.1	3.0	2.9		
Fe-C-S	100 ppm				48.9		38.0		31.4			26.7	19.3	21.5	16.2	15.6	13.2	12.0	7.5			
Fe-C-Si-Cr	0.1 pct						16.7	11.5	9.7								7.1	5.7		5.8		
Fe-C-Si-Cr	0.5 pct			42.0	30.0	25.8	24.3	14.5	10.1	8.4		8.0										

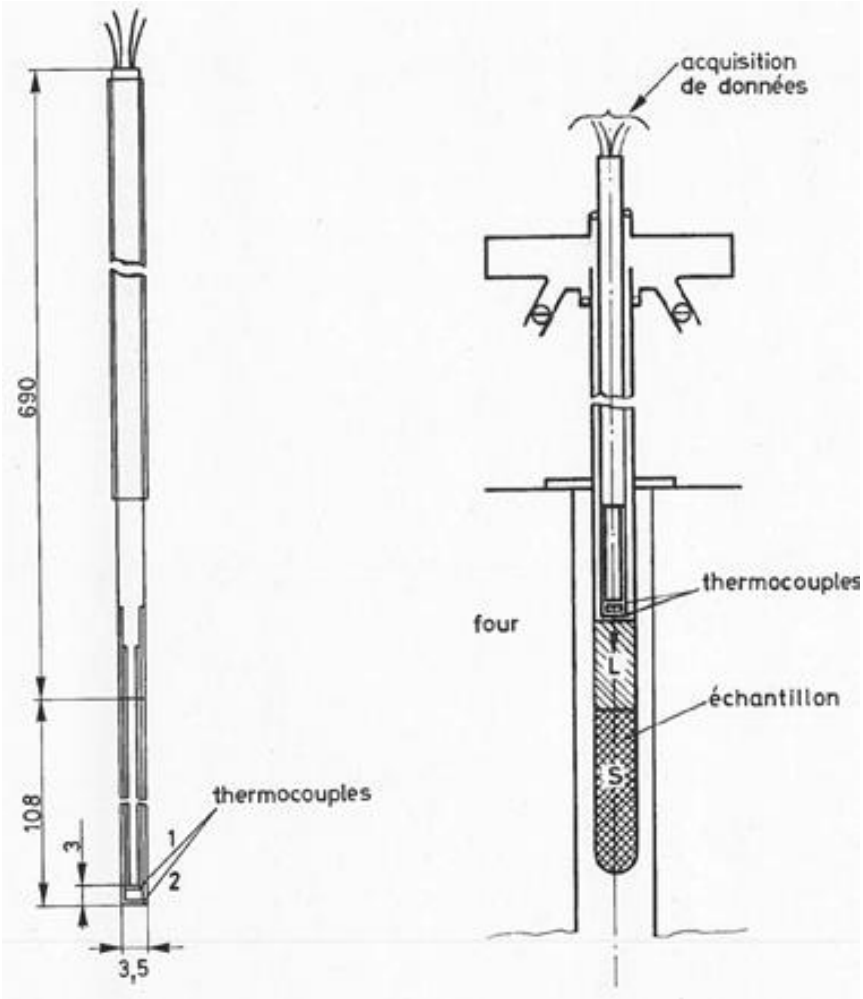

Figure 6: Thermocouple system developed for determining temperatures of gray and white iron eutectic [16].

Table 2: Growth temperatures for Fe-C alloys at different solidification rates [8]

Alloy		Growth Temperatures (°C) DTA[12] (~0 μm/s)	3.3 (μm/s)	16.7 (μm/s)	33.3 (μm/s)	67.7 (μm/s)	100 (μm/s)	K_s (K $\mu m^{-1/2}$ $s^{1/2}$)
Fe-C eutectic		1154.5	1148.8	1140.6			1121.6	3.3
Fe-C-Si	0.1 pct	1155.2	1147.3	1141.5	1132.9	1125.8	1116.7	3.7
	0.5 pct	1157.0	1149.6	1139.5	1133.5	1124.8	1114.8	4.1
Fe-C-P	100 ppm	1153.9	1148.4	1138.8	1133.4	1125.2	1119.3	3.5
	0.1 pct	1152.1	1149.7	1147.8	1144.9	1141.2	1140.1	1.2
Fe-C-Cr	300 ppm	1153.3	1148.2	1140.2	1134.4	1128.1	1122.3	3.1
	0.5 pct	1148.5*	1148.2*	1147.4*	1147.2*	1146.8*	1146.1*	0.24*
Fe-C-Mn	0.1 pct	1154.2						3.2**
	0.6 pct	1150.6	1146.3	1139.3	1135.4	1130.4	1124.3	2.6
Fe-C-Ti	100 ppm	1153.5	1146.8	1138.8		1124.8	1116.8	3.6
	0.2 pct	1150.3	1144.4	1133.0	1124.5	1116.8		4.4
Fe-C-Al	500 ppm	1156.6						3.5**
	0.2 pct	1159.5	1151.3	1142.9	1134.1	1122.5	1117.2	4.3
Fe-C-S	50 ppm	1154.9						3.7**
	100 ppm	1152.1					1111.5	4.1
Fe-C-Si-Cr	0.1 pct	1153.9						3.4**
	0.5 pct	1150.9		1135.7			1113.7	3.7

*White eutectic
**Linear regression (effect of the alloying element assumed to be proportional to the composition)

Hypoeutectic cast iron has been shown to vary from spheroidal to compacted to flake graphite depending on the growth velocity, temperature gradient at the solid/liquid interface and cerium concentration [17]. The variations in structure that can form are shown in Figure 7. The regular graphite morphology of gray iron is lamellar; however with increased Ce composition and/or growth velocity, the structure changes.

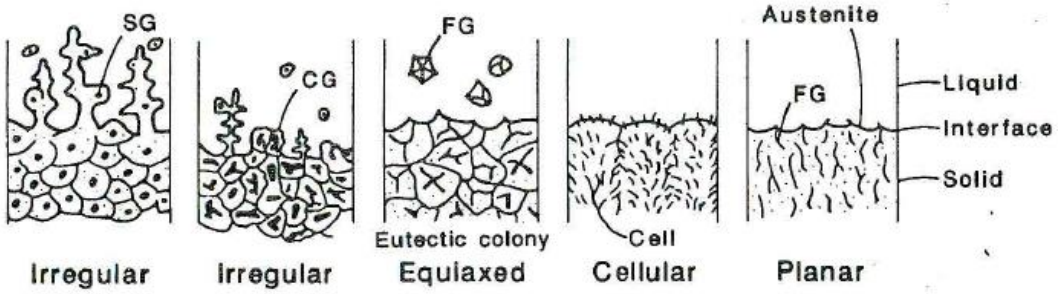

Figure 7: Possible morphologies of the solid-liquid interface and of the graphite in cast iron [17]

Researchers have also taken the challenge to develop analytical models of complex material systems. The objective has been to predict how a material will behave in a specific environment before manufacturing since it is more efficient and cost

effective. Laurentiu Nastac [18], developed a mathematical model for equiaxed and columnar solidification, including the instability of the solid/liquid interface. In the work done by Nastac, an analytical model was successfully created to calculate the solute redistribution of dilute binary alloys. The important application of the model is the prospect of obtaining accurate values of some thermophysical properties of dilute binary alloys at various conditions [18].

Additional information on modeling structure parameters of Fe-C eutectic growth can be found through the work of Guzik and Kopycinski [19] on the irregular eutectic growth (faceted/nonfaceted crystallization) in Fe-C and Al-Si alloys. The Magnin-Kurz theory of irregular eutectic growth was modified to understand the physical mechanism motivating the crystallization process. Through the use of the model calculations of parameters from the nonfaceted and faceted interfaces, can be acquired. Parameters such as the interlamellar spacing and the protrusion of the nonfaceted phase were attained through experimental and modeling results. The results showed that modeling is an extremely useful tool to predict the behavior that a certain material demonstrates in certain conditions [19].

1.2. Problem Statement and Objectives

The different structures that cast iron can form as a function of growth velocity and composition have been reported by various researchers. However, the expected structure of directionally solidified gray iron based on composition and growth velocity is still a debate between researches since the properties that will determine the morphology

are extremely sensitive. There is still much to understand in order to be able to predict the behavior in cast iron, particularly when additional alloying elements are present.

In this research, eutectic gray iron will be characterized using stereology and an experimental method to determine the growth temperature of the samples will be developed. This will aid in determining the values of spacing at different velocities and compositions in order to develop a model to better understand cast iron. The work will also focus on validating and optimizing a recently developed automated MATLAB code to create a time efficient and objective way of measuring eutectic spacing when the spacing is highly irregular. The samples used are gray iron samples with different compositions of C, Si and Mn at velocities close to or below the critical velocity for obtaining austenite dendrites.

2. MATERIALS AND METHODS

2.1. Sample Manufacturing and Processing

Gray iron samples were prepared from Sorel pig iron, high purity C, SiC and FeMn melted in a 100 lb induction furnace at high temperature. Alloying elements were added directly to the melt in the induction furnace. Carbon and sulfur content was measured using LECO, while other elements were determined using electric arc spectrometer. Once the correct chemical composition was achieved, individual samples were collected with evacuated glass tubes. The bubble in the tube opened up when submberged into the molten iron then the change in pressure caused the metal to fill the tube. Figure 8 shows a picture of the evacuated glass tubes used for acquiring samples.

Dimensions of the evacuated glass tubes are 5.5 mm outside diameter (OD), 3.5 mm inside diameter (ID) and 15 cm of length.

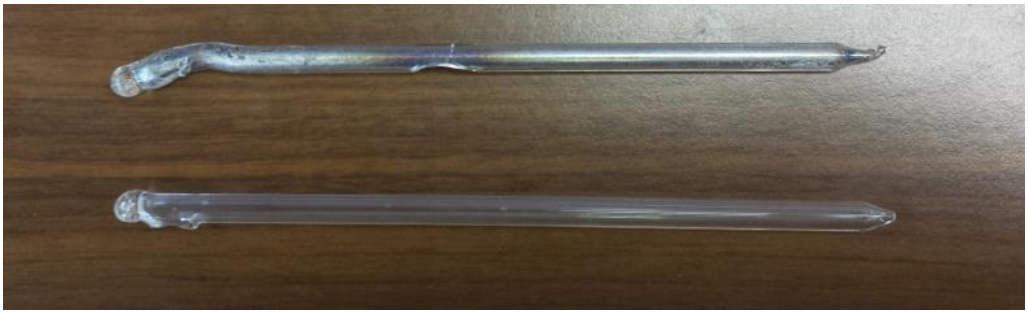

Figure 8: Evacuated tube used for collecting the gray iron samples for directional solidification

A total of five different alloys were created; with varying C, Si and Mn concentration. The compositions can be seen in Table 3. The table includes the carbon equivalent for each composition, calculated with Equation 1. The goal was to make each composition as close as possible to the eutectic composition (4.3 wt% CE). The Sorel pig and alloy #1 are hypereutectic, while alloys #2, 3, and 4 are somewhat hypoeutectic.

Table 3: Compositions of the samples taken from the induction furnace given in weight %. Final row indicates carbon equivalent for each composition

Sample ID	Sorel Pig	#1	#2	#3	#4
C	4.52	3.84	3.42	3.57	3.45
Si	0.21	1.67	2.07	2.01	2.08
Mn	0.025	0.074	0.095	0.593	0.669
P	0.008	0.017	0.015	0.012	0.016
S	0.009	0.007	0.010	0.009	0.011
Mo	0.058	0.060	0.061	0.062	0.062
Ni	0.149	0.141	0.135	0.136	0.138
Cu	0.065	0.079	0.087	0.096	0.092
CE	4.59	4.39	4.11	4.23	4.13

Directional solidification experiments were carried out in a vertical Bridgman furnace with MoSi heating elements and a water-cooled copper chill block (see Figure 9). The set temperature of the furnace ranged from 1230°C to 1300°C. Samples were placed inside a cylindrical alumina closed bottom crucible. The alumina crucible used had dimesions of 5 mm ID, 7 mm OD and 45 cm in length or 6 mm ID, 1 cm OD and 45 cm in length. Because the pieces of metal obtained from the evacuated glass tubes were thinner than than the crucibles, multiple pieces were inserted for processing. Adding multiple samples to the crucible ensured that there was sufficient samples to fill the crucible with an appropriate quantity of metal. Solidification velocities of 0.5 μm/s to 10 μm/s were used for the specimens that were processed through the Bridgman furnace. Moreover, all the processed samples were completed under an argon atmosphere to avoid any molecule or element in the air reacting with the molten metal.

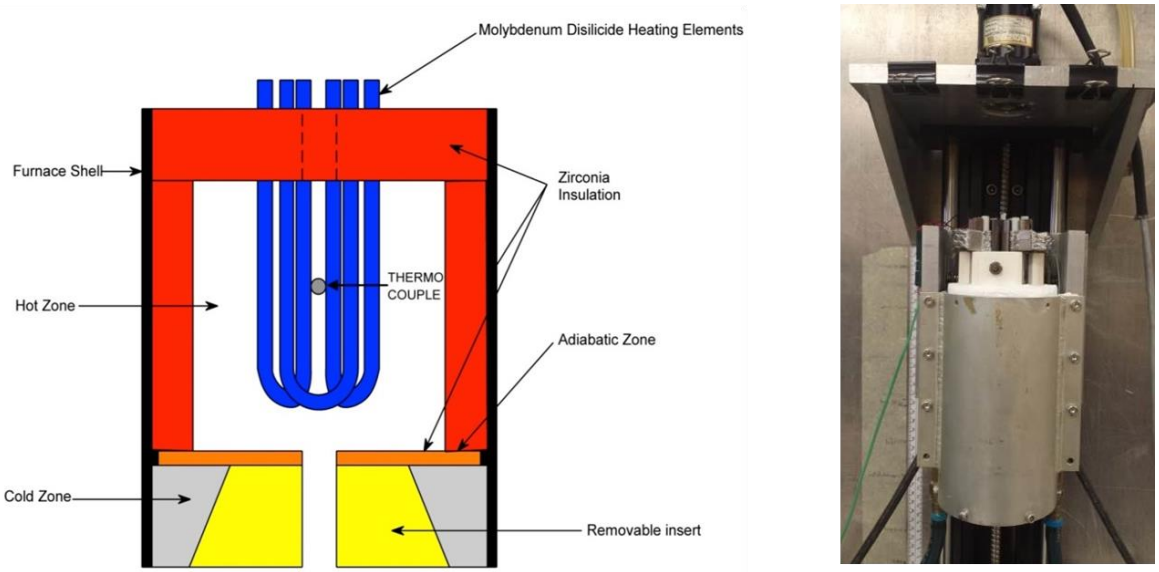

Figure 9: (Left) Schematic of furnace. (Right) Photo of furnace

The thermal gradient inside the furnace was measured using two fine gage sheathed thermocouples inserted directly into a sample during solidification. Figure 10

shows a graph of the temperature profile within the furnace when the furnace temperature was set to 1230°C. The arrows indicate the expected solidification temperature and the corresponding position in the furnace at which solidification occurred. Figure 11 shows the measured thermal gradient as a function of furnace position, indicating a thermal gradient of around around 4°C/mm in the region where solidification was occurring. Section 2.3 discusses about the arrangements used for experimentation as well as additional information about the thermocouples and other materials used.

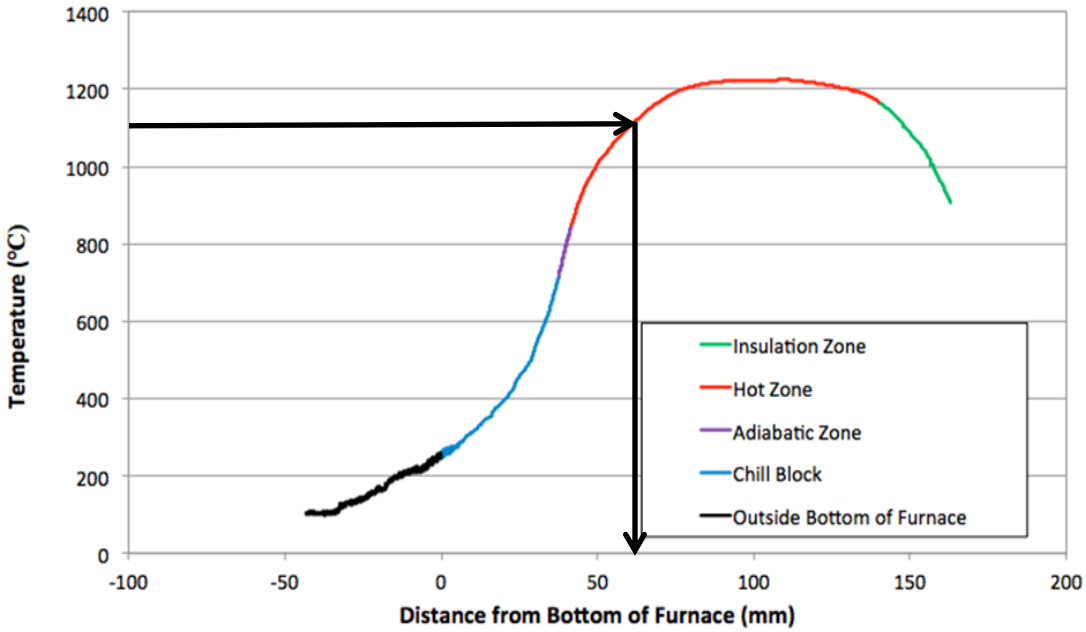

Figure 10: Temperature as a function of position graph for thermal profiling (Arrows show the solidification temperature and the corresponding position in the furnace)

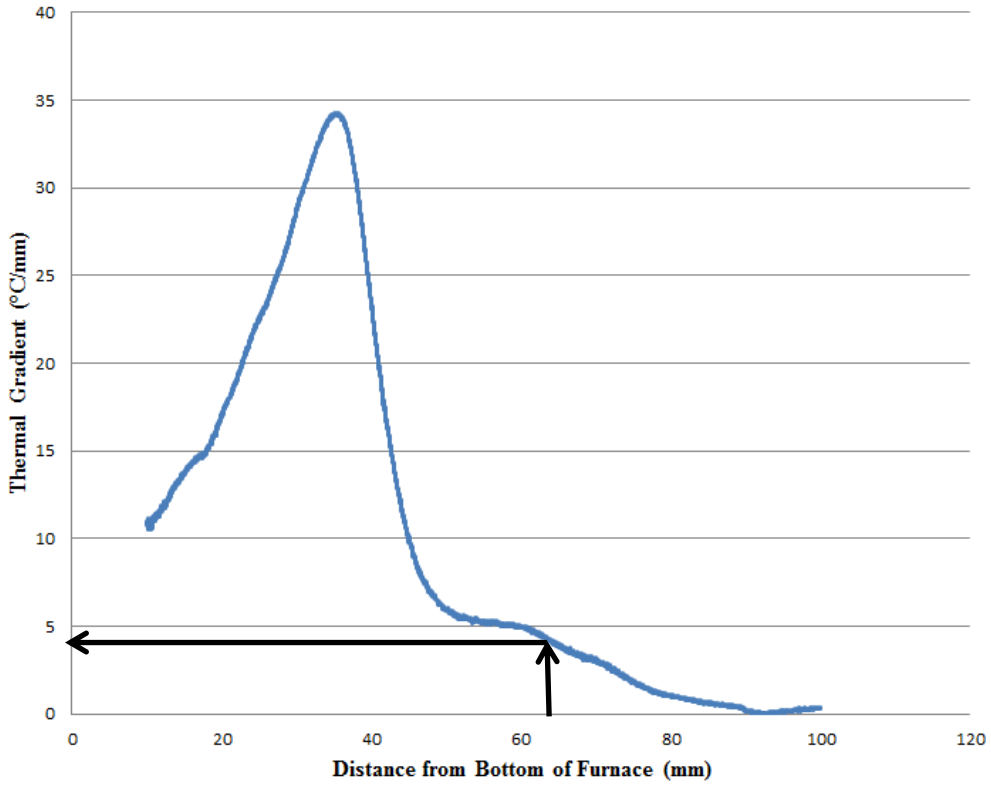

Figure 11: Thermal gradient as function of position (Arrows show the position where solidification occurs, as found in Figure 8, and the corresponding gradient.)

Processed samples were approximately 7-9 cm in length and 5mm in diameter. The samples were mounted longitudinally in epoxy resin for polishing and examination. Samples were polished with the grinding equipment with the roughest sandpaper of 60 grit and increasing grit until 1200 grit; lastly the samples were also polished with one micron diamond paste. Optical images taken at 100X were used to measure the average and minimum graphite spacing. Maximum spacing is not reported since the samples used in this project contained austenite dendrites and primary graphite, which made determining maximum spacing difficult. The standard line intercept method was used: drawing a line perpendicular to the direction of the graphite and dividing the length of the line by the number of graphite flakes intercepted. For each sample, a minimum of 25

measurements was taken from a minimum of 5 images. An example of such measurements is shown in Figure 12.

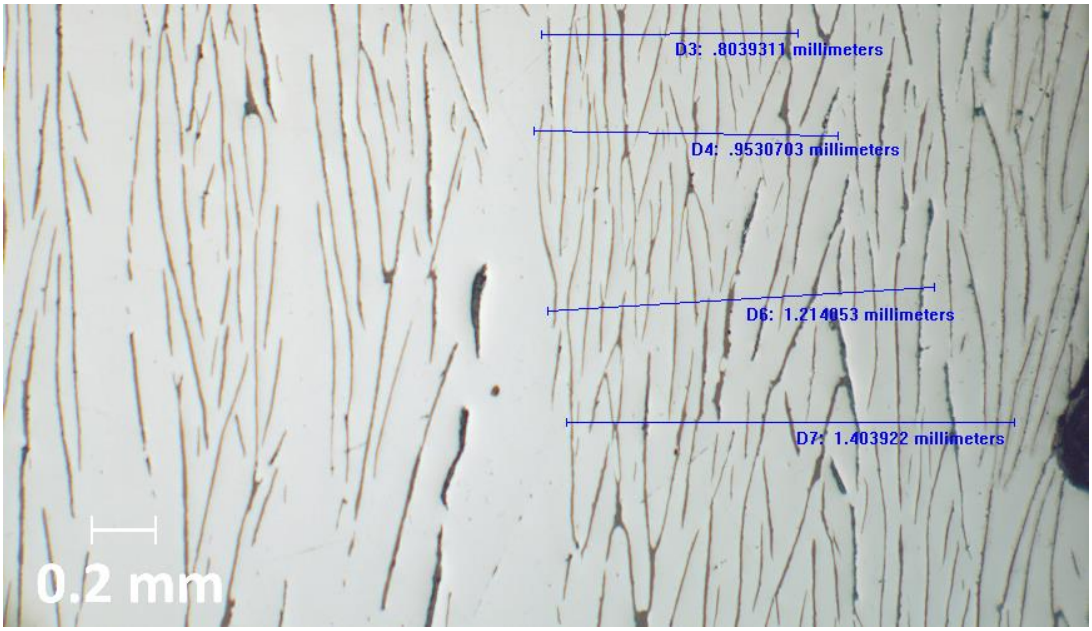

Figure 12: Manual calculation of graphite spacing in a relatively well aligned region for alloy #2 at 0.5 µm/s (Magnification: 40X)

2.2. Automated MATLAB Process

Because of the irregular nature of the graphite-austenite eutectic, measuring eutectic spacing in gray iron is not trivial; and the measured spacing can depend highly on the exact placement of lines by the investigator. In order to decrease subjectivity and increase the number of measurements to improve the statistical averages, measurements were also taken using an automated technique recently developed using MATLAB [20] (outlined in Figure 13). Optical microscope images with the highest level of alignment were selected. For each image, a specific region was selected by the user. Each region was thresholded to create a binary image. Then two settings were adjusted to ensure that the correct spacing was measured. First, spacing was measured starting from each pixel of the image along lines set at user determined angle increments. Second, the total line

length was determined by the number of crossings specified by the user. Figure 14 shows a visual representation of the definition of crossing according to the code.

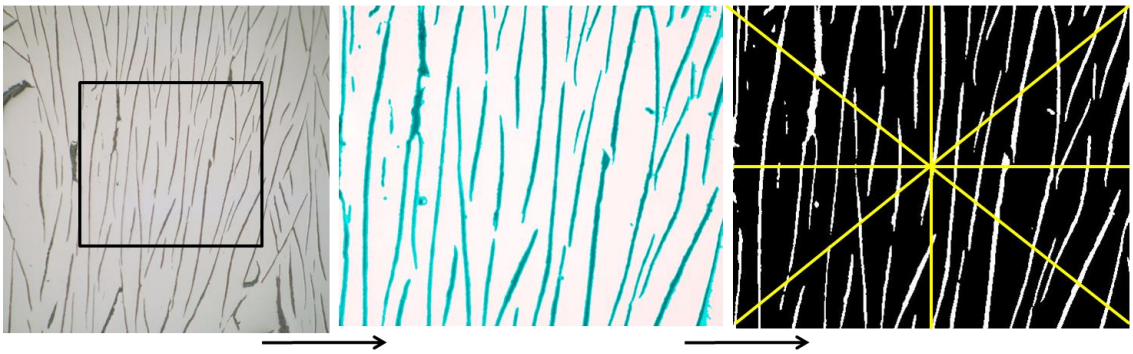

Figure 13: Automated stereology method: (Left) Region selected for measurement. (Center) Thresholded image overlayed in the original image. (Right) Lines drawn by program to calculate minimum spacing at each pixel (45˚ angle increment which is four angles/lines)

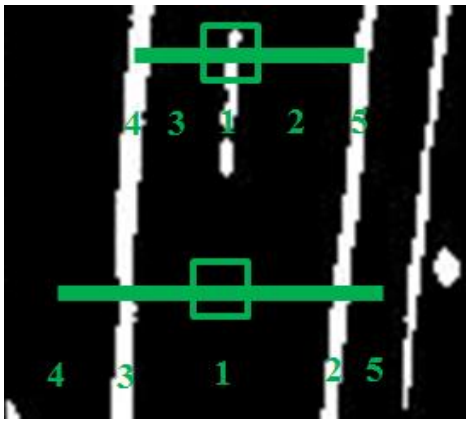

Figure 14: Thresholded image of crossings in the flake graphite; a total of 5 crossings are represented for both a black and a white starting pixel (white area represents flake graphite while dark area represents austenite)

The program then determined the line length depending on the crossings and calculated spacing of the dark and light regions. The measured spacing was compared for all angles/lines, and only the minimum spacing was recorded. The line with the minimum spacing is most closely perpendicular to the flakes and should be considered the true spacing for that area. The minimum spacings for all regions analyzed was collected and

used to determine the minimum and average spacing for that sample. A comparison of manual and automated spacing values was completed to validate the automated code.

2.3. Solid/Liquid Interface Temperature

In order to determine the temperature of the solid/liquid interface, a setup of two thermocouples separated by a gap of approximately 3 mm were used. Fine gage (0.005 inch) type S thermocouples were manually threaded through Omegatite 450 alumina sheaths. The thermocouples were used to measure the change in temperature and thermal gradient when the solid/liquid interface passed the thermocouple tips. Different arrangements of thermocouples were considered for experimentation, and each of them were attempted at individual experiments. The thermal data was recorded for the entire directional solidification experiment with a Personal Daqview Excel Add-in.

The first systems of thermocouples were attached to the side of the alumina crucible bonded with OMEGABOND 600 high temperature cement. The powdered cement was mixed with water at the ratio specified by the instructions of the cement. After mixing, a cotton swab was used to apply the cement to the side of the alumina crucible and then bond the sheathed thermocouples to the crucible. The cement was left to dry from 18-24 hours at room temperature, then oven dried for four hours at 82˚C and an additional four hours at 104˚C, as instructed by the guidelines of the OMEGABOND 600 for elevated temperature experiments. The disadvantage of the mentioned system is that the thermocouples were not in contact with the molten metal to get the most sensitive thermal data.

The second setup involved using an open bottom alumina crucible. The same system of sheathed thermocouples was used; but to avoid direct contact between the

thermocouple wire and the molten metal, the tips of both thermocouples were covered with the same high temperature cement, mixed at a very high powder to water ratio. The thermocouples then were inserted through the bottom of the crucible, and the bottom was sealed with high temperature cement. This arrangement puts the themocouples in most direct contact with the melt for increased sensitivity, but can result in molten metal leaking from the crucible which can damage the thermocouple system and even the inside of the Bridgman furnace.

The last arrangement used was insulating the sheathed system of thermocouples with a small alumina crucible and then inserted the alumina crucible containing the thermocouples directly into the melt from the top of the crucible. This arrangement suffers from the disadvantage of the sample being processed open to atmosphere and not under argon. In addition, although the molten metal completely surrounds the inner crucible containing thermocouples, the thermocouples are still not in direct contact with the melt. Figures 15-17 show the three setups for acquiring interface temperature data. For both the second and third setup, the samples were contained inside the slightly larger alumina crucible, in order to accommodate the sheathed thermocouples.

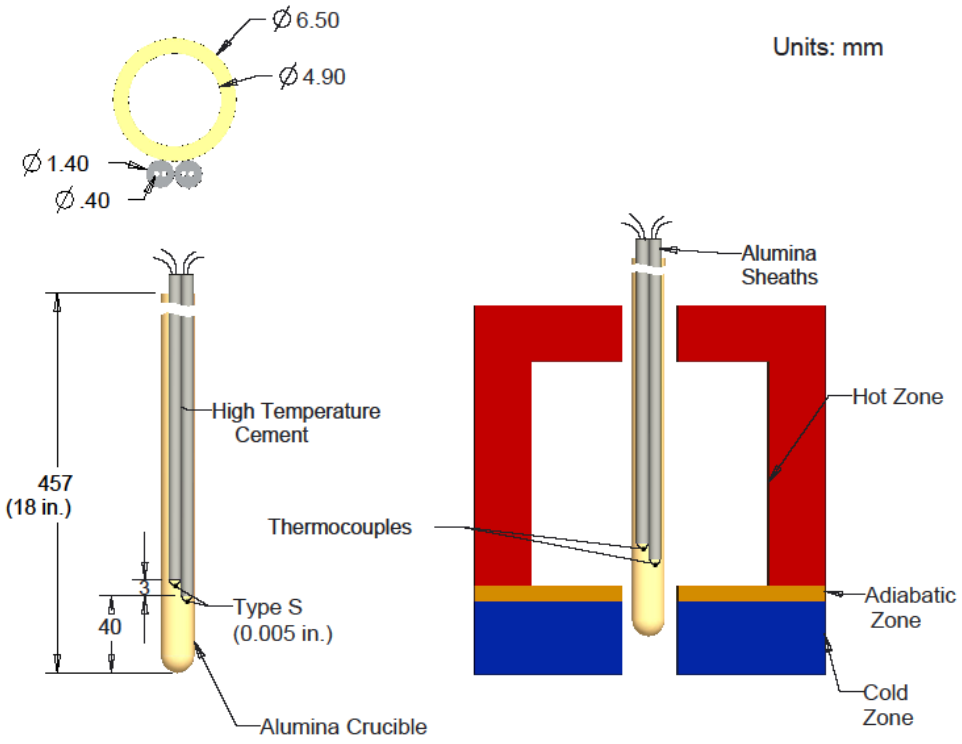

Figure 15: First setup of thermocouples system (Thermocouples attached to the side with high temperature cement)

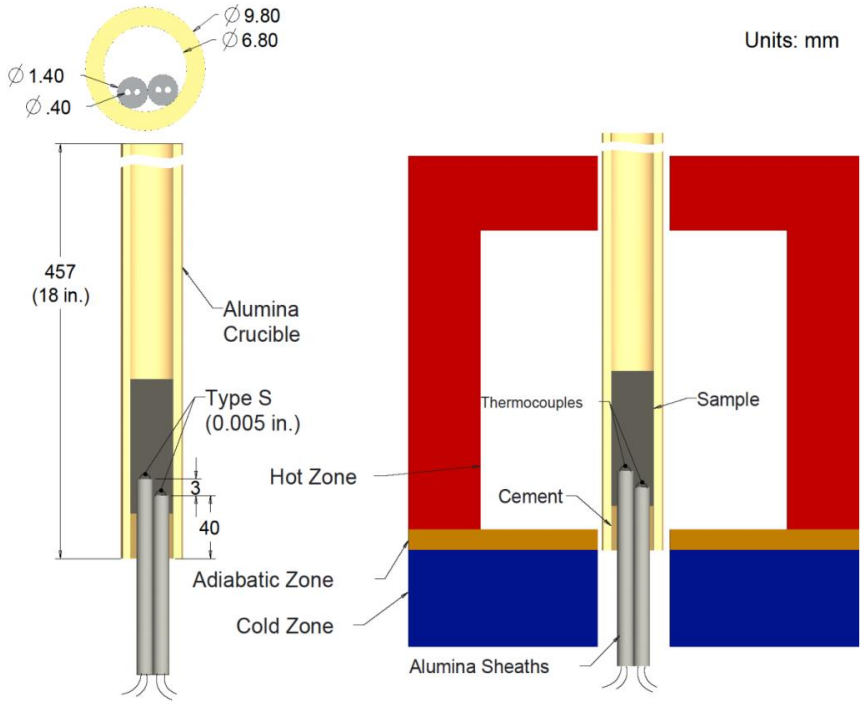

Figure 16: Second setup of thermocouples system (Thermocouples inserted through bottom and sealed with high temperature cement)

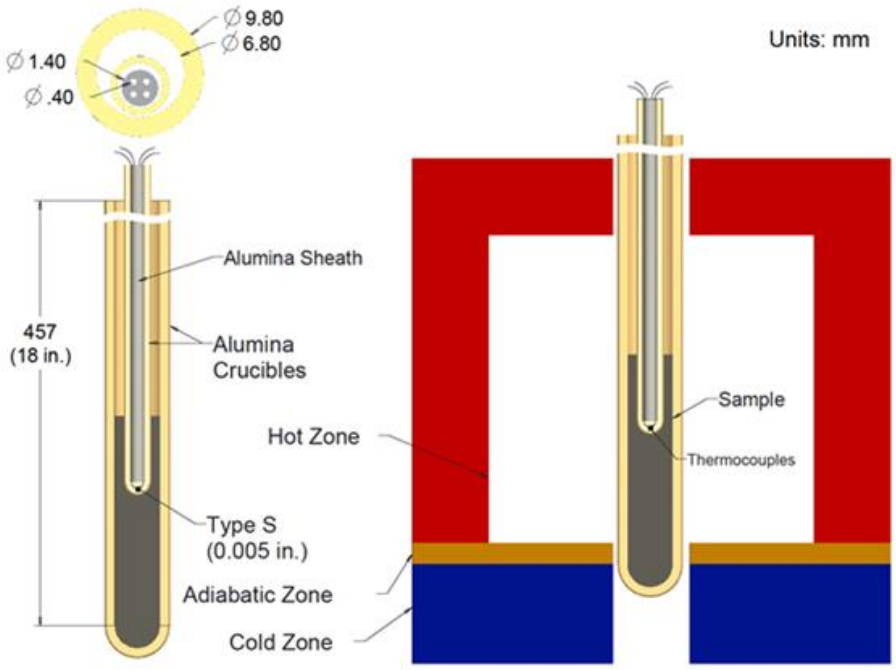

Figure 17: Third setup of thermocouples system (Thermocouples inserted from top of crucible to the melt)

3. RESULTS AND DISCUSSION

3.1. Effect on Spacing due to Composition and Velocity Changes & Results

For this project, the effects of composition and growth velocity were included in the results. Figure 18 shows how the effect on the spacing of the directionally solidified samples. Each sample was solidified at 0.5 μm/s in an upward direction. The picture of gray iron base (4.42% CE) and #1 (4.36% CE, 1.7% Si) show what may be primary graphite. This sample has a hypereutectic composition which means primary graphite is expected to be present in the structure. The rest of the samples have hypoeutectic compositions and must be below the critical velocity value. For this reason, the samples show neither dendrites nor primary graphite. The samples also show differences in both the thickness of flakes and the level of alignment. Figure 19 shows higher magnification images of the flake graphite of the five different samples.

Stereology spacing measurements were made for the five gray iron samples and the results are shown in Table 4. The results show that as silicon and manganese is added to the gray iron, the spacing decreases slightly. This is consistent with modeling results, which suggest that spacing is dependent on the amount of alloying element as well as the diffusivity of the element [23].

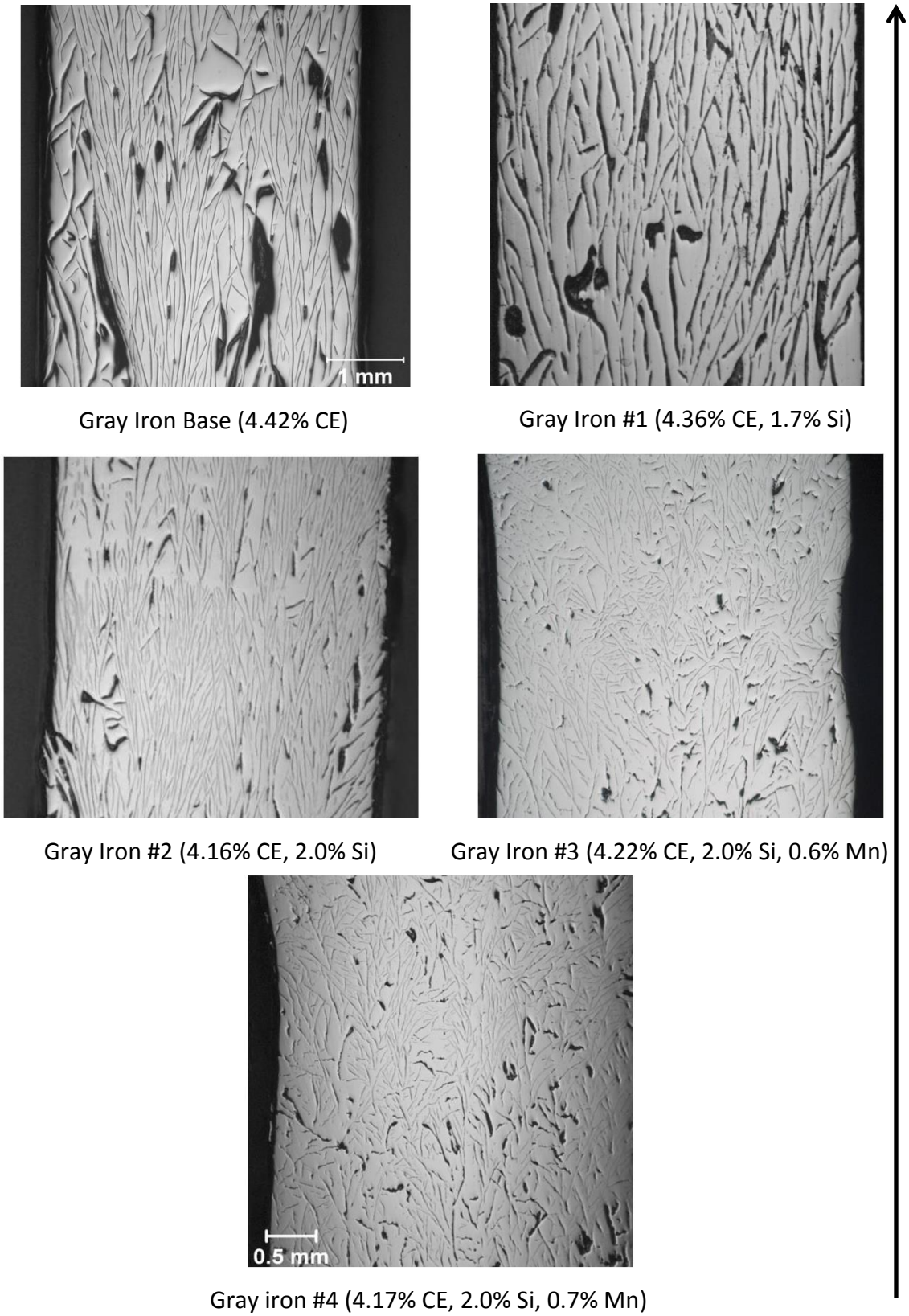

Figure 18: Representation of the five gray iron samples directionally solidified at 0.5μm/s (Samples approximately 4.5 cm from bottom of furnace; magnification: 16X)

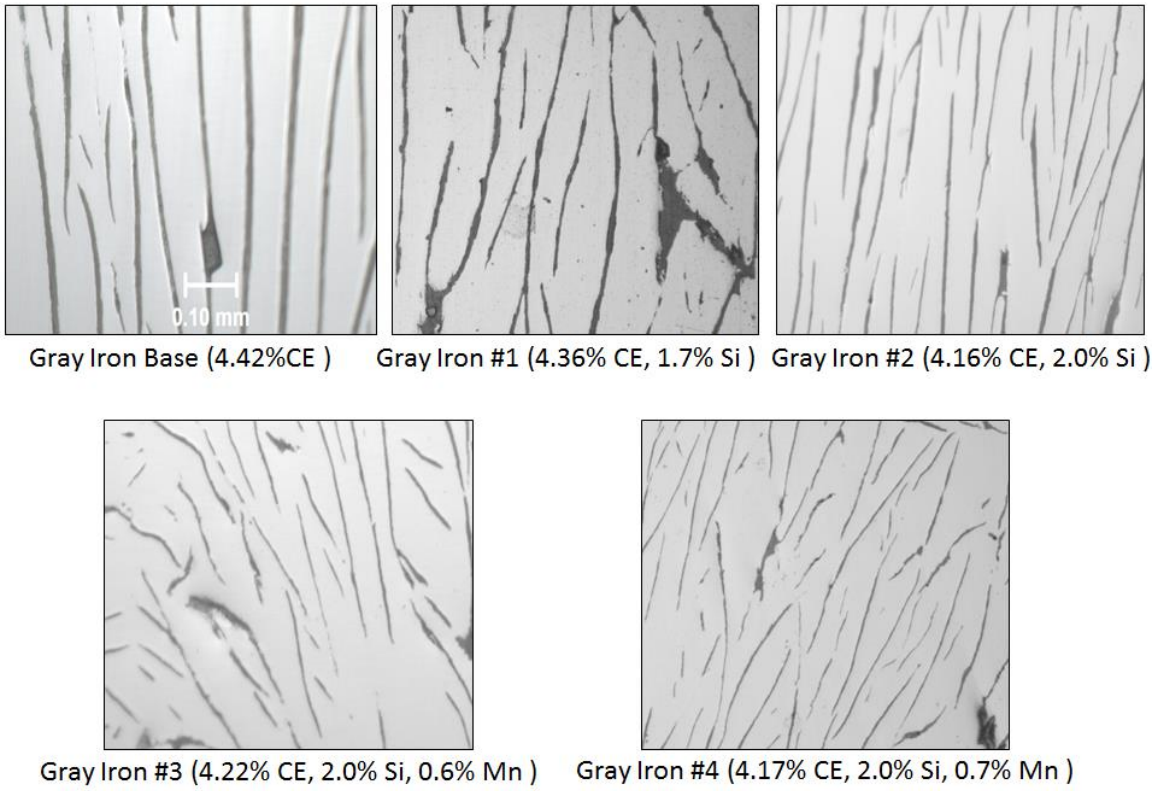

Figure 19: Higher magnification of the flake graphite for the gray iron samples (Magnification: 65X)

Table 4: Manual spacing results of gray iron samples directionally solidified at 0.5 µm/s

Sample	Spacing (µm)	Std Dev
GI Base (4.42% CE)	56.3	4.2
GI #1 (4.36% CE, 1.7 Si)	58.6	5.8
GI #2 (4.16% CE, 2.0% Si)	47.0	7.1
GI#3 (4.22% CE, 2.0% Si, 0.6% Mn)	40.3	5.9
GI #4 (4.17% CE, 2.0% Si, 0.7% Mn)	42.7	2.6

A study of the growth velocity effects on spacing was also completed for one composition. Figure 20 and 21 show pictures of the effect changing the growth velocity on the spacing in gray iron sample #1. Image in Figure 19 is the structure obtained with a velocity of 0.5 μm/s. The bottom image shows a single sample where the velocity was changed from 1.0 to 5.0 μm/s during solidification. The spacing decreased drastically with increased velocity. Results also show that flake graphite at higher velocities is thinner and ceases showing directionality. In addition, austenite dendrites are present at higher velocity even though the composition is hypereutectic. Because no dendrites are present in the 0.5 μm/s sample, this indicates that the critical velocity is between 0.5 μm/s and 1.0 μum/s. Furthermore, primary graphite can be seen in the sample because of the hypereutectic composition of the sample.

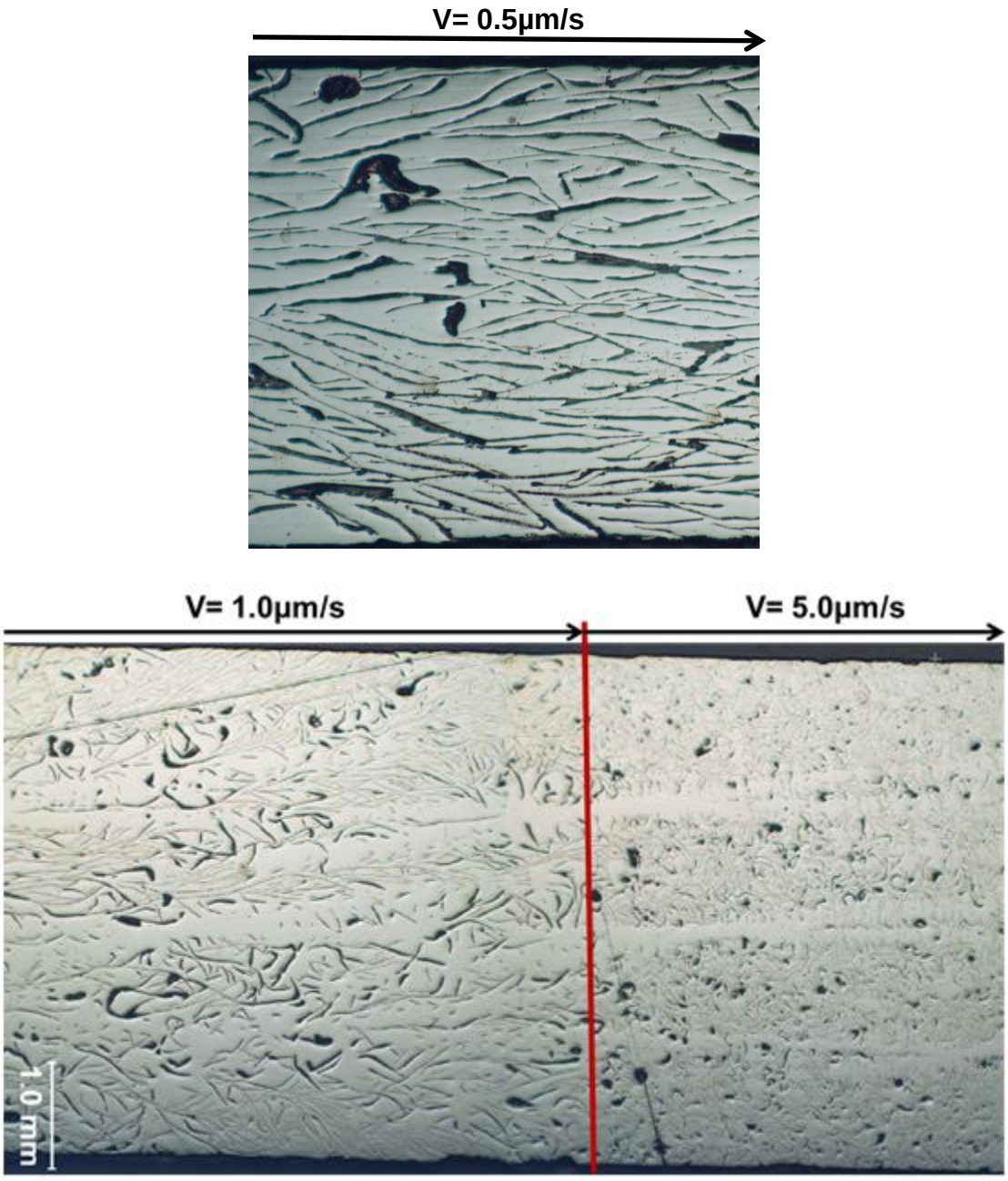

Gray Iron #1 (4.36%CE, 1.7 Si)

Figure 20: Effect on spacing due to growth velocity change in gray iron (Magnification 15X)

Figure 21: Higher magnification of the flake graphite at different growth velocities (Magnification: 27X)

The spacing values obtained from this work were compared to previous experimental values reported in literature. Figure 22 shows a plot comparing both sets of values; it is noticeable that the current samples have larger spacing than the ones reported by Magnin and Kurz [8]. The primary difference between literature and current work is the additional alloying elements. Clearly the amount of alloy has a direct effect in spacing. The Magnin and Kurz values show the change in spacing with velocity predicted by the Jackson and Junt equation, but their data does not show any consistent effect of the alloying elements at the low concentrations used. Additional velocities with the current alloys are necessary to determine a trend.

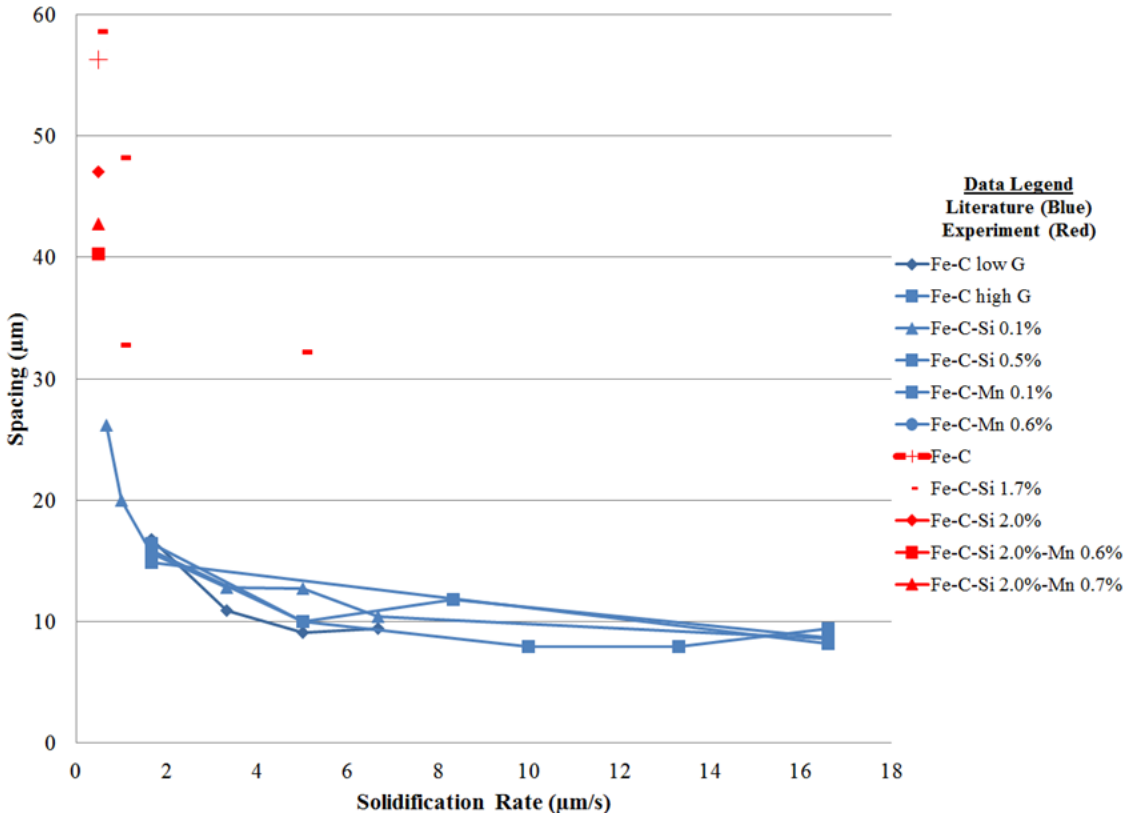

Figure 22: Experimental spacing values compared to literature (from [8])

The Jackson and Hunt constant (K) from the equation $\lambda = K/\sqrt{V}$ was calculated from the data for gray iron sample #1 (Fe-C-Si 1.7%). Spacing values were reported by Magning and Kurz and K values were determined for the reported solidification rates shown in Table 1. Experimental spacing values were determined for three different solidification rates and compared to those given by literature. K values were determined by converting the Jackson and Hunt equation into the linear equation y = mx; y represents the spacing (λ) while x represents one over the square root of the velocity of solidification ($\frac{1}{\sqrt{V}}$), and the slope m represents the K value of the equation. Figure 23 shows the results of K values for this experiment and literature.

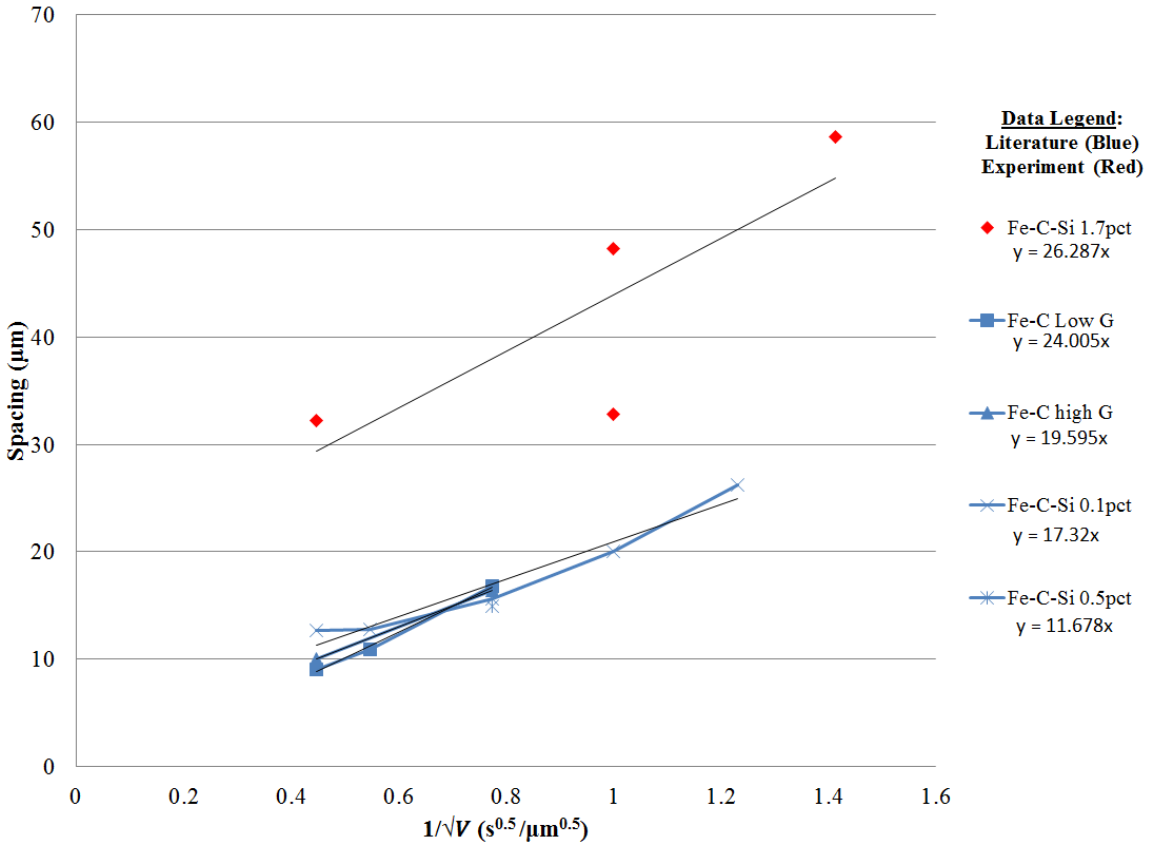

Figure 23: Experimental K values compared to literature (from [8])

The literature shows that K decreased with an increased alloy and thermal gradient. A similar trend was seen in the experimental data from gray iron #1 Experimental data from gray iron #1 in this project showed that there is an increase in the higher percentage of silicon concentration. The value of K for the gray iron #1 gives an approximate 26.3 $\mu m^{1.5}/s^{0.5}$; this value is close to the literature value of Fe-C low G which is 24 $\mu m^{1.5}/s^{0.5}$. This suggests that there is a clear effect on the constant K for a higher percentage of additional alloys. Both literature and experiment data collected show that the slope increases with increasing value of $\frac{1}{\sqrt{V}}$.

Primarily, longitudinal sections were analyzed for spacing measurements for the different gray iron samples. In addition, four transverse sections of gray iron #1 were

examined in this project. Figure 24 shows the representative image of the four sections investigated. The sections were taken starting from the bottom of the sample and were spaced at 1 cm apart from each other. The bottom of the sample was labeled section 1 and the top (farthest solidification distance from the bottom) was labeled section 4. By the images shown, it is possible to see that there maybe a difference in spacing between the sections. Manual spacing measurements were made for the transverse sections shown in the picture. Table 5 shows the spacing results with the standard deviations. Because of the increase in directionality of the graphite as distance from the bottom, the measurements were difficult to make consistently. However, it does appear that the spacing was longer in the sample 3 cm from the bottom. Section 1 shows more areas without flake graphite than the other sections. These areas are considered austenite dendrites that were formed at the beginning of solidification. However, since the velocity of solidification was below critical value, eventually the dendrites disappear. Additionally, section 4 shows the highest directionality of flakes out of all the structures.

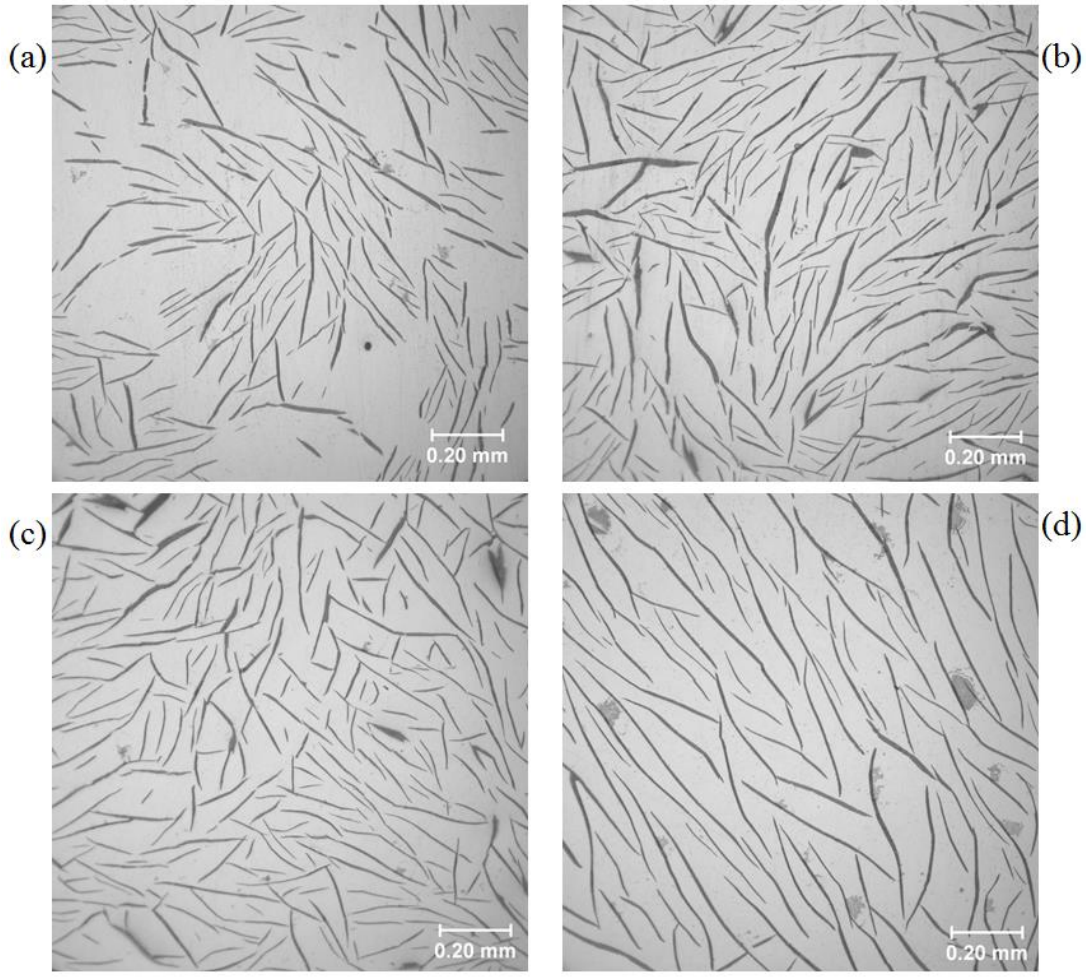

Figure 24: Transverse sections for Gray iron #1: (a) bottom of sample, (b) 1cm from bottom, (c) 2 cm from bottom, and (d) 3 cm from bottom (Sample solidified at 0.5 µm/s)

Table 5: Manual spacing measurements for transverse sections of gray iron #1 directionally solidified at 0.5 µm/s

Distance from Bottom (cm)	Spacing (µm)	Std Dev
0	34.8	3.6
1	43.8	1.7
2	44.9	3.2
3	50.3	2.8

The table shows that as the material was being directionally solidified the spacing grew as solidification distance increased. The spacing value from section 4 approaches

the longitudinal spacing. The longitudinal section manual stereology measurement for gray iron #1 was 58.6 μm, measured approximately 4-5 cm from the bottom of the sample. The transverse section that was 3 cm from the bottom of the sample has a spacing of 50.3 μm. Only four transverse sections of the entire sample were analyzed, and it could be possible that if more sections at longer distances had been measured the spacing would eventually remain steady at the value that was determined for longitudinal sections. The effect of solidification distance on longitudinal spacing was not systematically measured. However, the results of the transverse image measurements indicate the importance of position within a sample.

3.2. MATLAB Spacing Code Parameter Study

An additional objective of the project was to validate an automated code that is in the process of being developed [20] in conjuction with this project. Once completed, the new code will serve as a more objective and time efficient method for calculating spacing measurements in irregular eutectics as well as other types of structures. A study was carried out to validate the code and determine the optimum parameters for spacing measurements. Angle increment and number of crossings were the two selected parameters to optimize the code. Gray iron alloy #2 solidified at 0.5 μm/s images were used because of their high degree of alignment, and gray iron #3 solidified at 0.5 μm/s images were used to test images with low alignment.

3.2.1. Angle Increment

The angle increment variable of the code refers to the degrees of rotation between each line at which spacing is measured fore each pixel. It is inversely related to the number of lines over which spacing is measured, i.e. if we use 60˚ increments then there

will be three lines drawn, at 0˚, 60˚ and 120˚. Figure 25 shows a thresholded image with spacing being measured for four different angle increments. While a smaller angle increment is expected to be more accurate, it also significantly increases the run time for the code.

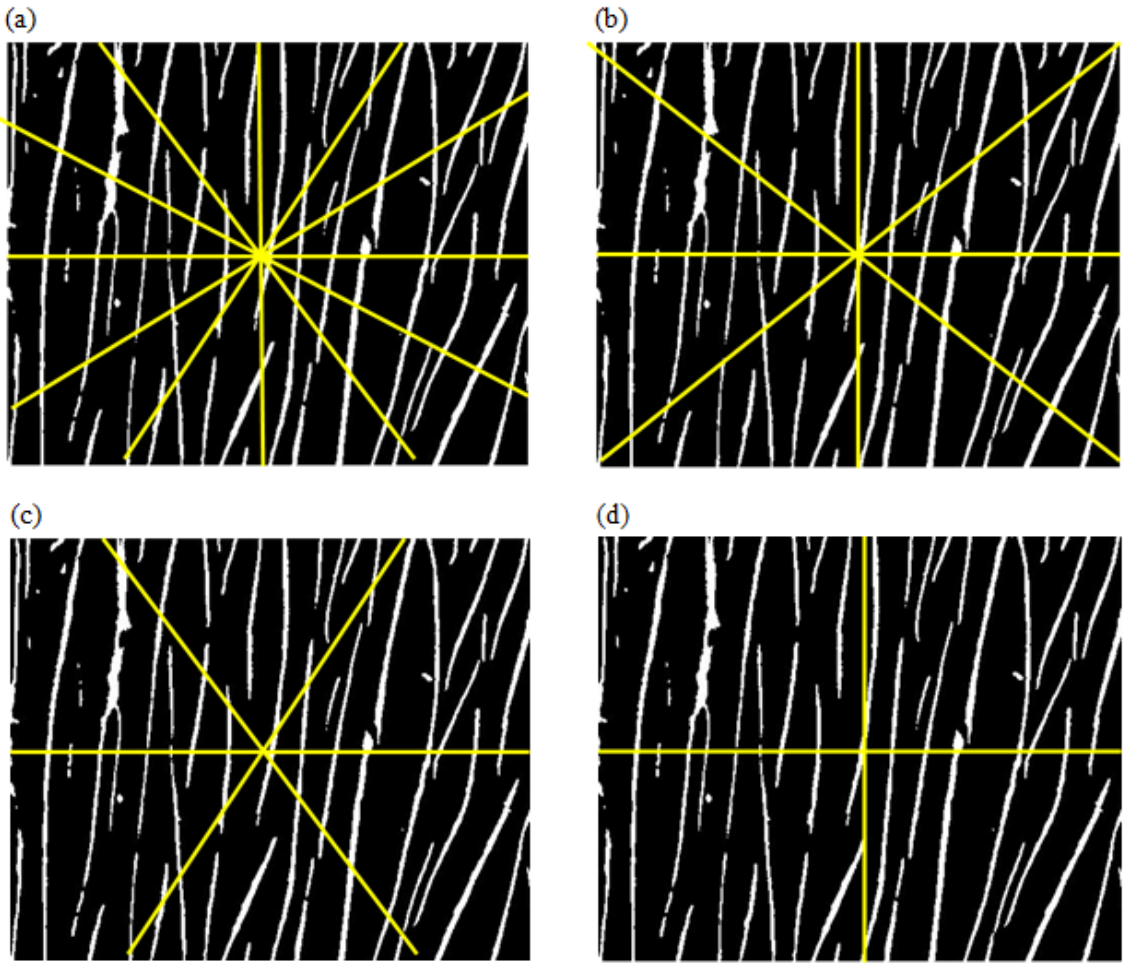

Figure 25: Thresholded picture of gray iron sample with (a) 30° (6 angles), (b) 45° (4 angles), (c) 60° (3 angles) and (d) 90° (2 angles) increment for gray iron sample #2 directionally solidified at 0.5 µm/s

Figure 26 shows the effect of angle increment on the spacing for samples with well aligned graphite. These results were obtained from line length set to 15 crossings. The figure shows that for the highly aligned pictures any of the angles used for the code would output accurate results. This is because the flakes were well aligned with the

vertical direction of solidification and the line that outputs minimum spacing is always expected to be the 0˚ line. However, the 30˚ angle (6 lines) was used for the purposes of this project, since with this angle it is evident that plenty of lines are being drawn over the image to calculate the correct spacing of the image. Some of the images that are being analyzed in the project are not entirely aligned in the vertical direction, and therefore more lines are needed at a lower increment to accurately determine the spacing of the flake graphite.

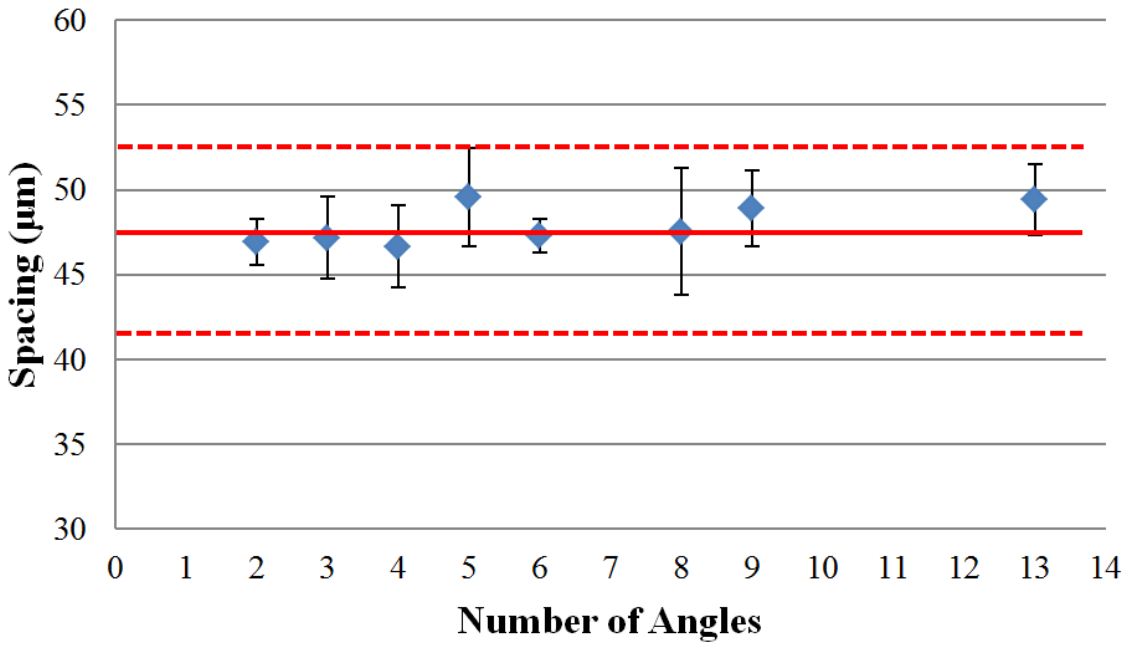

Figure 26: Scatter of spacing versus number of angles for well aligned flakes (Error bars represent the 95% confidence interval; solid red horizontal line represents the manual value of spacing)

An additional study of angle increments was done with the least aligned sample that was manufactured. Results showed that the spacing value decreased as the number of angles sampled increased, approaching the value measured manually. This means that taking larger angle increments would then not be drawing the line in where the actual minimum spacing is located. Figure 27 shows these results.

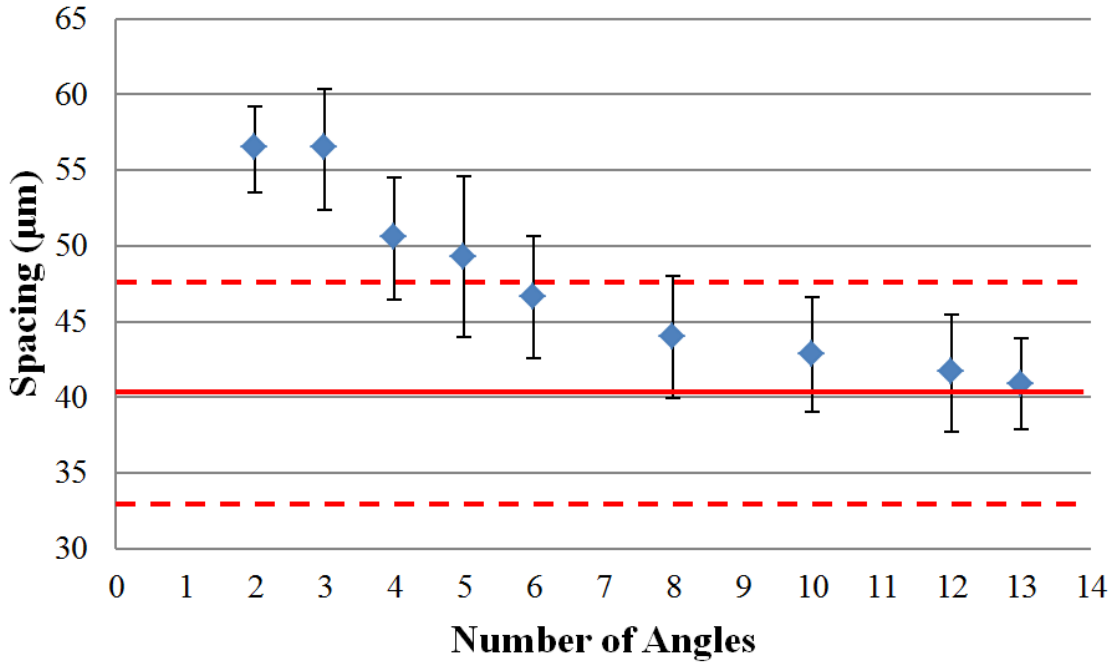

Figure 27: Scatter of spacing versus number of angles for least aligned flakes (Error bars represent 95% confidence interval; solid red horizontal line represents the manual spacing value)

3.2.2. Crossings

The other variable that was used in the MATLAB code is the number of crossings (line length). The crossings of the code is an important variable to consider since it is what will determine how many flakes are being taken into account when it comes to estimating the spacing of the gray iron. In order to have accurate values of spacing, the number of crossings has to be within range of the quantity of graphite that is present in the picture when using the code. This means that if the code has a low number of crossings then it is averaging over a smaller number of flakes. Figure 28 shows the results on the parameter study of the MATLAB code with crossings. These results were obtained with a setting of 8 angles.

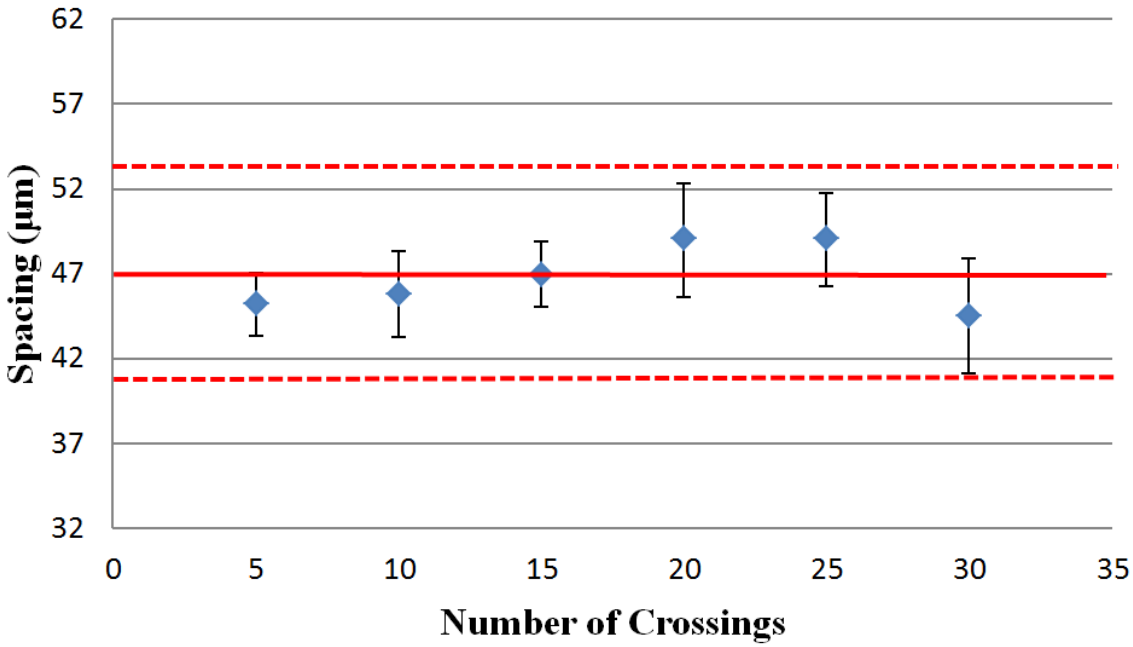

Figure 28: Scatter of spacing versus number of crossings for well aligned flakes (Error bars represent 95% confidence interval; solid red horizontal line represents the manual spacing value)

It is noteworthy by looking at the spacing results with the 95% confidence intervals, that the MATLAB code is giving precise values for the crossings. Nonetheless, there is a notable decrease of spacing value for 30 crossings. This suggests that there are a limited number of crossings in which the image itself will output accurate values. After the limit has been reached it will decrease the spacing values considerable or it will output not a number (NaN). To support the results shown earlier, an additional study of crossings was completed for the least aligned sample, shown in Figure 29. The results in this figure were obtained with a setting of 13 angles. The results show that the spacing decreases as number of crossings is increased, with a particularly sharp drop above 20 crossings, where the returned results become incorrectly low. In the next section, the comparison of between manual and automated methods will be discussed with the optimized values of crossings and angle increment.

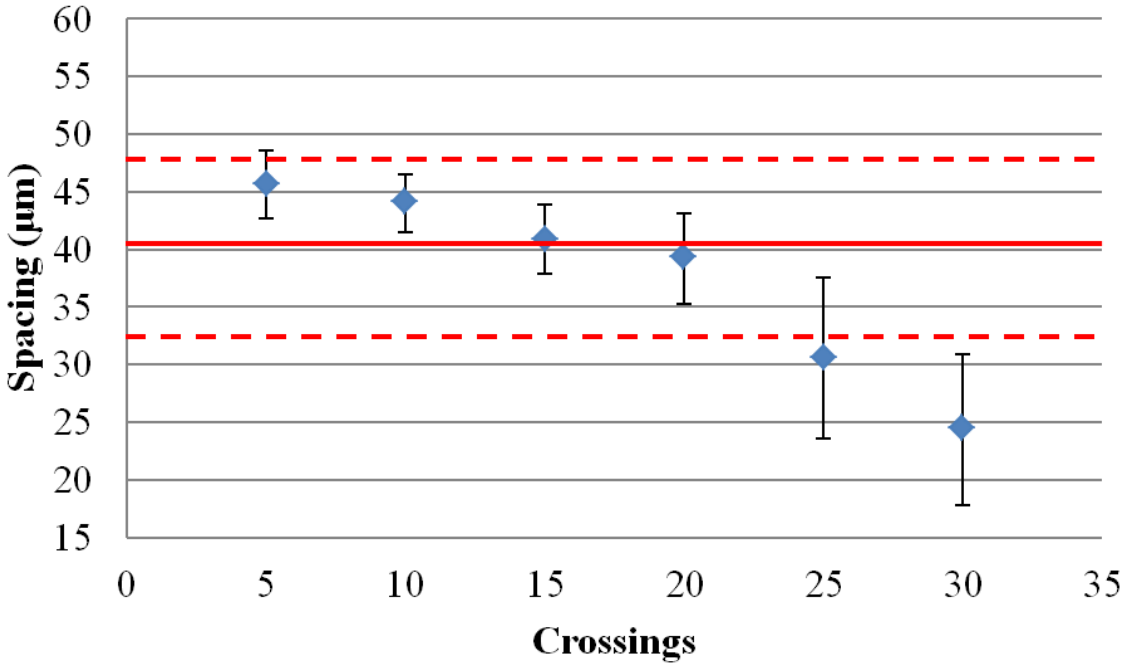

Figure 29: Scatter of spacing versus crossings for least aligned flakes (Error bars show 95% confidence interval; solid red horizontal line represents the manual spacing value)

The parameter study results concluded that the optimum parameters for determining the accurate value of spacing with the automated algorithm was six angles (30˚ angle increment) with 15-20 crossings for well aligned flakes of graphite; while for least aligned flakes the ideal values were 13 angles (13.8 angle increment) with 15-20 crossings.

3.3. Comparison of Manual and Automated Results

In order to determine the accuracy of the MATLAB code, manual versus automated spacing measurements were compared. The automated values were produced with optimal values of crossings and angle increment parameters. The angle used for the study was set at 30˚ increment while the number of crossings usually was set at 25 crossings. However, this value was sometimes decreased depending on the quantity of

flakes that were present in the pictured analyzed. As mentioned in section 3.2.2, if the crossings are over or under estimated, the code will output erroneous values of spacing. In Figure 30 a bar graph is shown comparing the spacing values for both automated and manual spacing measurements of all the gray iron samples directionally solidified at 0.5 μm/s. Additionally, the graph shows calculated spacing values of the model developed by Catalina and Vorhees (represented by triangular shaped points) [21]. Comparing both sets of values showed that the model is accurate for close to eutectic and/or hypoeutectic composition, while for hypereutectic composition the model proves ineffective. The possible explanation for the difference of value for the hypereutectic composition is due to the existence of primary graphite in the sample that affects spacing measurements.

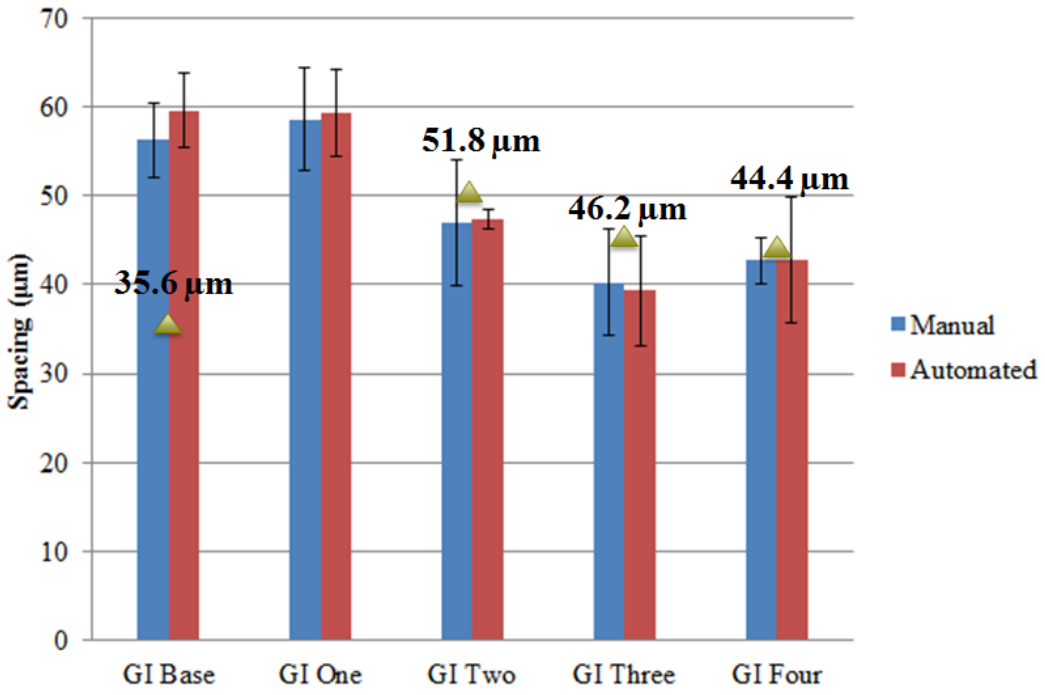

Figure 30: Spacing of manual and automated spacing methods (Error bars represent standard deviation; triangle shaped points are spacing measurements from reference [21])

The data shows that the values of automated and manual spacing measurements have very similar values. The results show that the automated MATLAB code with the

selected optimized parameters accurately measures graphite spacing. On the other hand, the error bars shown in the figure are a representation of the standard deviations for the respective samples on manual and automated processes. It is noticeable that for the first three gray iron samples (Base, #1 and #2) the standard deviation is smaller for the automated process. The last two gray iron samples (#3 and #4) show a higher standard deviation for the automated process, which is a reflection of the lower degree of alignment in these samples. The reason for this result can be explained because of the effect of composition in spacing. Sample #3 and #4 have higher manganese content than the other samples, which will affect spacing and it is thought that the manganese could be having an effect on the ranges in spacing that are being taken into account when performing spacing measurements. For higher manganese percentages in the gray iron samples, the flake graphite is being formed with a wider range of spacing over the material. Even though that standard deviation for both samples are giving higher than expected, the average values of spacing are giving within the range of the actual spacing values, which shows that the automated MATLAB algorithm validated to this point is an effective method for objective and time efficient results. Table 6 shows the values of manual and automated processes being compared; it also shows the percent difference for all the samples studied in this experiment. In the table, negative difference error percentages are shown because in the original formula no absolute value is used in the difference. By doing this it will be clear to see if the values that the automated MATLAB code is outputting are being over or under estimated. Looking at the results, it is clear that the percentages of error difference are low. These results prove that the MATLAB code is an objective and efficient way to acquire spacing measurements.

Table 6: Manual and Automated Spacing measurements for gray iron samples solidified at 0.5 µm/s

Sample	Manual Stereology Spacing (µm)	Std Dev	Automated Stereology Spacing (µm)	Std Dev	Error %
GI Base	56.3	4.2	59.6	4.1	-5.9
GI One	58.6	5.8	59.4	4.9	-1.3
GI Two	47.0	7.1	47.3	1.1	-0.6
GI Three	40.3	5.9	39.4	6.2	2.3
GI Four	42.7	2.6	42.7	7.1	0.1

With the validated algorithm it was possible to also acquire additional data from the analyzed images. Flake graphite volume fraction and thickness was determined for all gray iron samples manufactured. Volume fraction measurements show that there is no abundant change in volume for the flake graphite as additional alloys are added to the iron-carbon alloy. However, the thickness of the flake graphite shows that there is a noticeable decrease in thickness as there is more additional alloy added to the alloy; Figures 31 & 32 show the volume fraction and thickness of the flake graphite for the gray iron eutectic alloys.

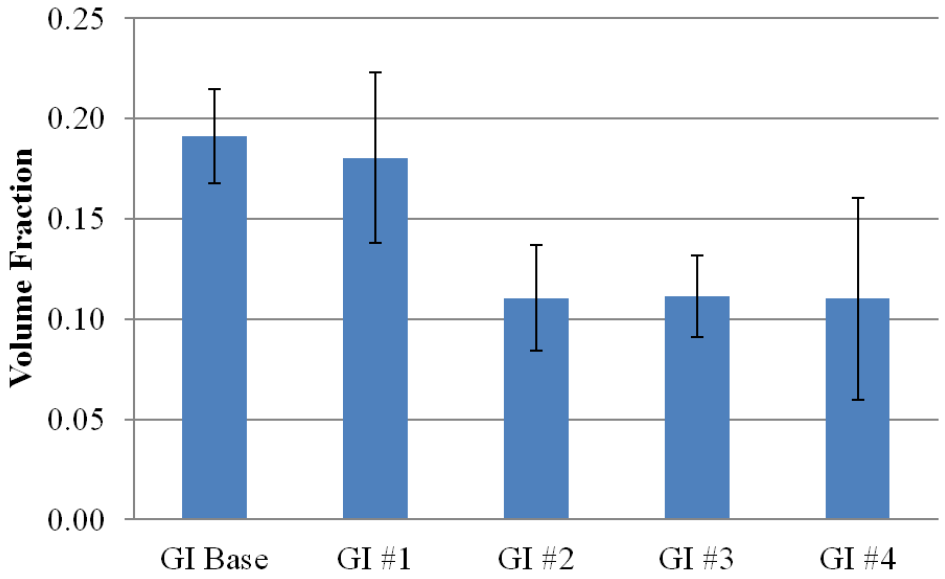

Figure 31: Volume fraction of gray iron samples directionally solidified at 0.5 µm/s

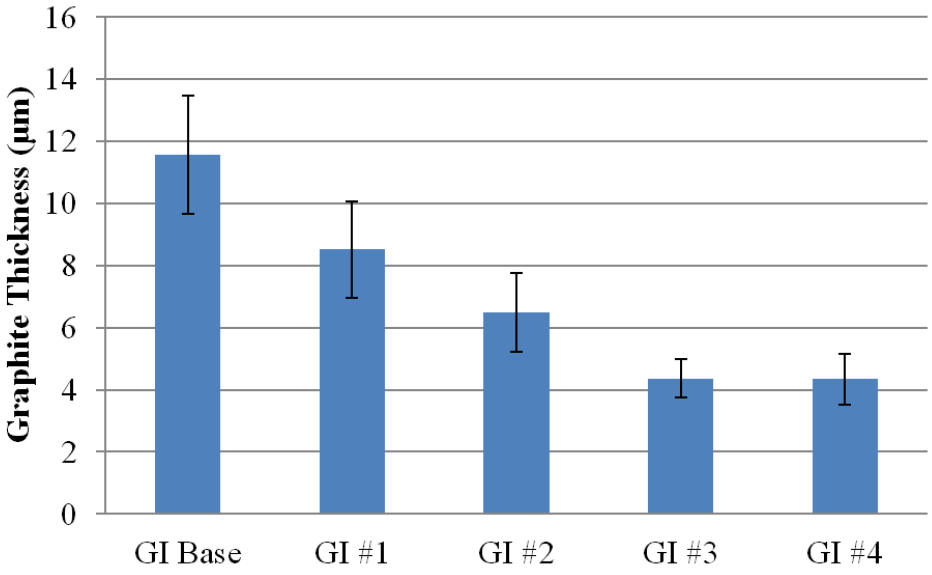

Figure 32: Flake graphite thickness of gray iron samples directionally solidified at 0.5 µm/s

3.4. Temperature Curve Data Analysis

Attempts to determine the solid/liquid interface temperature were performed for this project. The temperature curve data for at least four samples was determined and analyzed, however the results given by the thermal data were inconclusive. Temperature values were analyzed in the ranges that the sample should start to solidify. However, no noticeable disturbances in the thermal data were discovered from the data acquired. Figure 33 shows the temperature versus time plot for gray iron alloy #2 directionally solidified at 3 µm/s with the third thermocouple setup shown in Figure 19; Figure 34 shows the temperature range where the gray iron sample was expected to solidify. In this figure, it is clearly visible that no noticeable change in slope for both thermocouples occured. One possible explanation for the inability to determine the solid/liquid interface temperature is that the solidification velocities used for experimentation are very small, so the heat is being extracted extremely slowly and changes to the temperature curves are not large enough to notice.

The ideal graph would show an evident disturbance in the temperature curve graph. The disturbace would be caused by the release of latent heat and the thermal conductivity difference of the material. Since a change in slope is expected when the solid/liquid interface passes through the thermocouples, the slope of both thermocouples was graphed in Figure 35. A clear change in both slopes is noticeable, indicated by the dips in the purple and green curves, when the bottom thermocouple is at 1130˚C and the upper thermocouple is at 1160˚C. However, if the changes were a result of the passing of the solid/liquid interface, they should be offset in time. Since these changes are occurring at the same time, a positive conclusion cannot be made.

The data is further analyzed in Figure 36, which shows the thermal gradient as a function of time. No events are obvious here either. The furnace was set to a higher temperature for this run (1300˚C) in order to push the solidification position into a higher gradient region of the furnace because it was hoped that this would emphasize any changes in slope. This set of data was collected using experimental setup #3, where the thermocouples were inserted into the melt from the top, shielded by a second alumina crucible. It is possible that the thermal conductivity of the crucible was sufficiently different from the melt that it interrupted the solidification front, causing the solid to advance from the first to second thermocouple almost instantaneously. It is also possible that the air gap between the melt and thermocouples was enough to make them insensitive to the solidification front. No complete cooling curve data was obtained from thermocouple setup #2, which places the thermocouples most directly into the melt and is the only setup to thermally isolate them. This remains for future work.

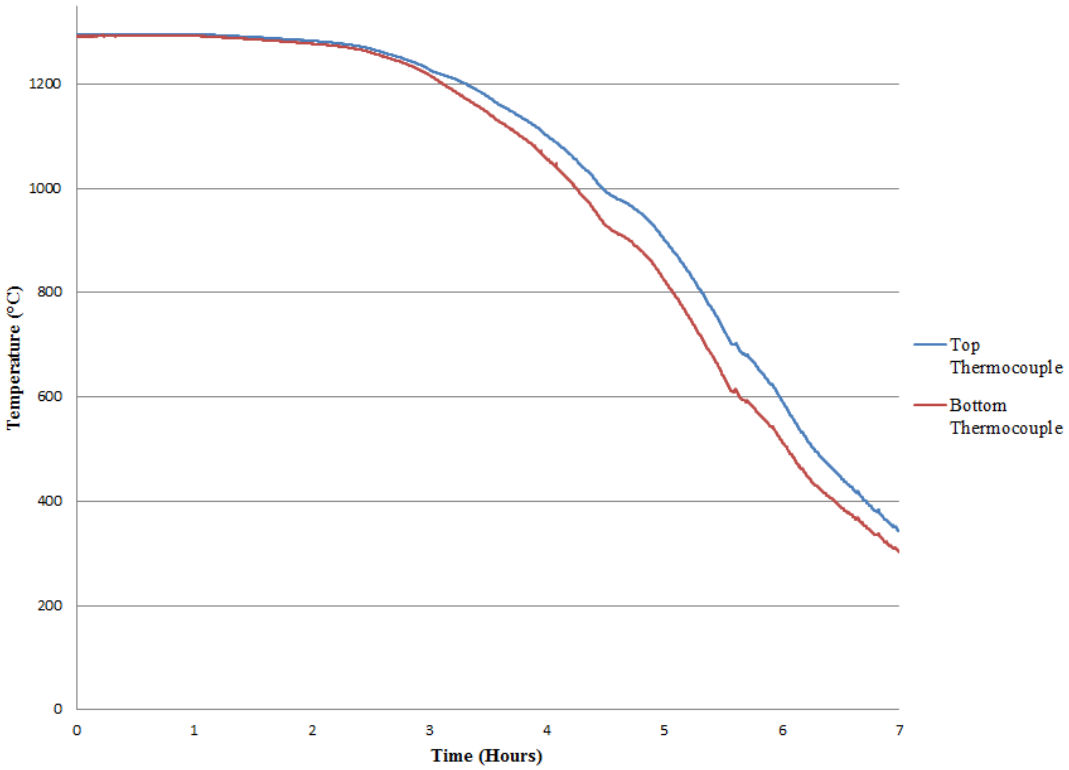

Figure 33: Temperature curve of gray iron sample #2 directionally solidified at 3 µm/s (Thermocouple setup #3 shown in Figure 19)

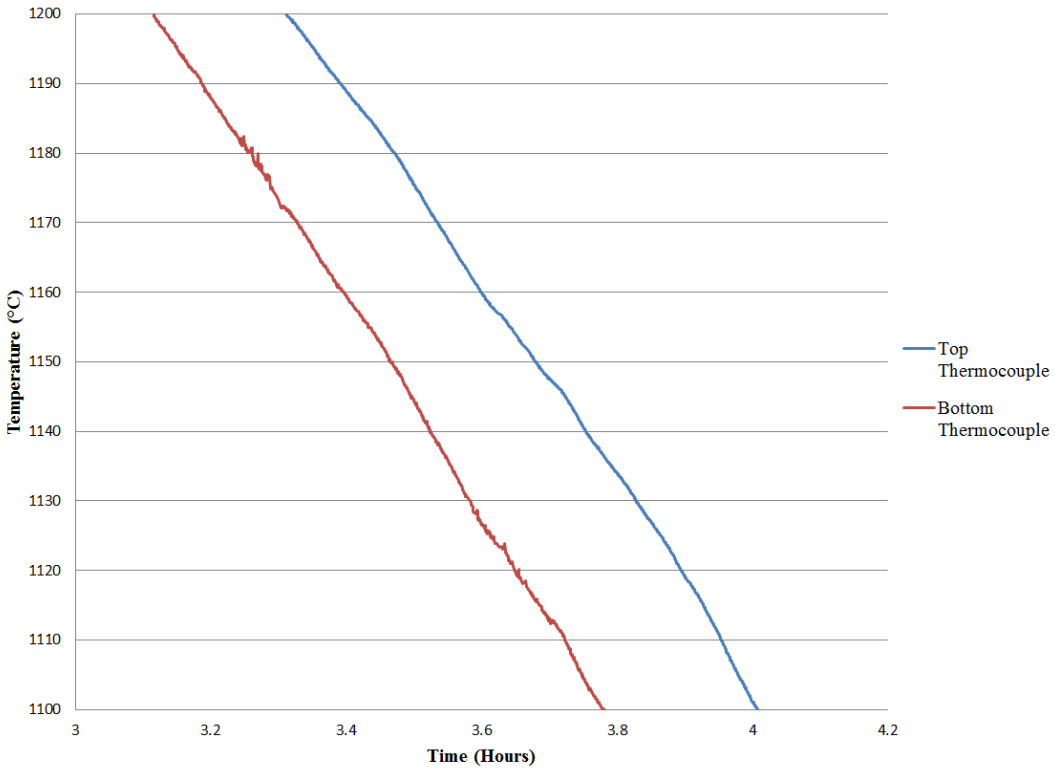

Figure 34: Thermal data recorded by thermocouples at the temperature ranges of expected solidification (Thermocouple setup #3 shown in Figure 19)

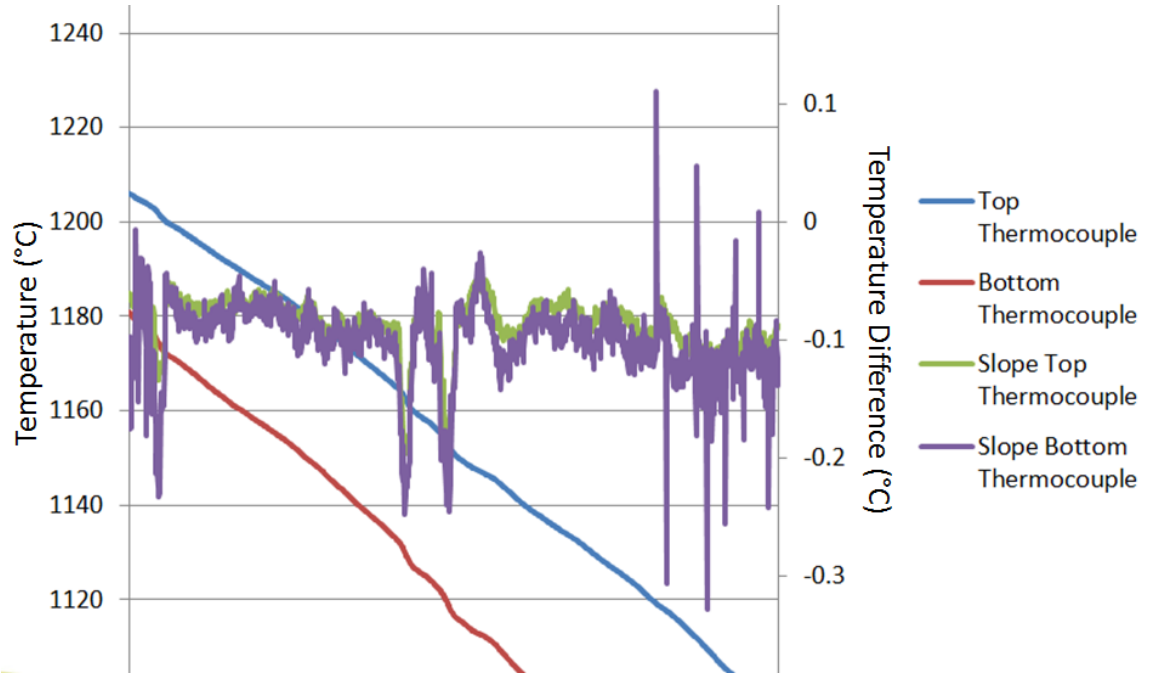

Figure 35: Slope scatter of bottom and top thermocouples (Thermocouple setup #3 shown in Figure 19)

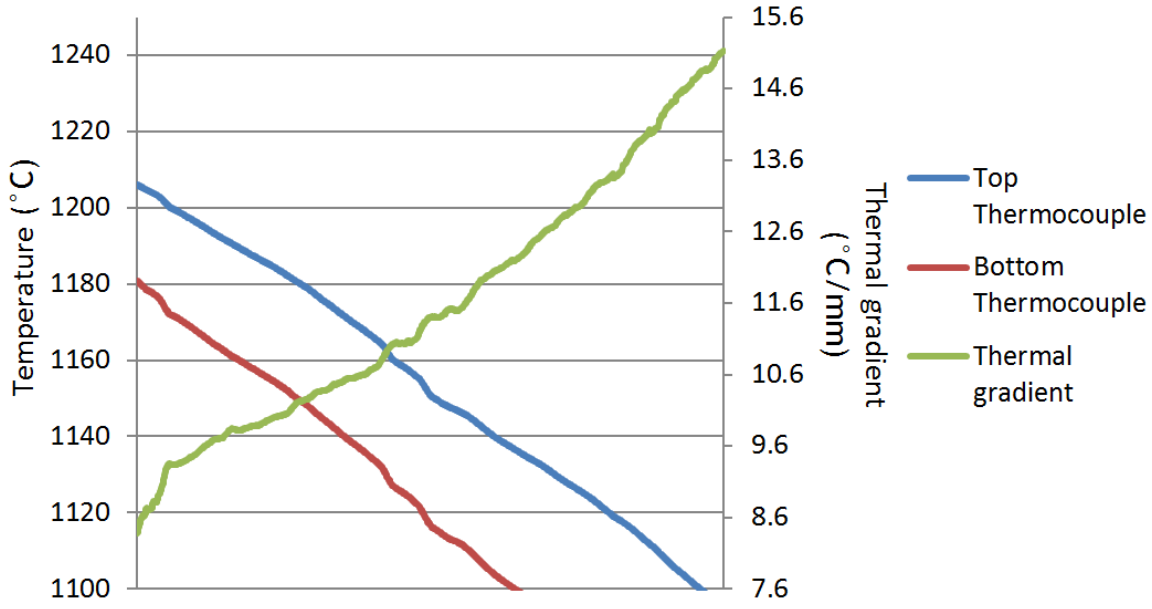

Figure 36: Thermal gradient graph for determining solid/liquid interface temperature (Thermocouple setup #3 shown in Figure 19)

3.5. Carbon Composition Analysis

A LECO element analysis machine was used to determine the amount of carbon and sulfur in the samples. The measurements were made before directional solidification and a limited number of the samples were also analyzed after. Table 7 shows the carbon percentages of the gray iron samples before directional solidification processing. Since the samples were manufactured in an induction furnace the content displayed in the table shows the percentage for the entire sample. Table 8 show the carbon content for two gray iron samples directionally solidified under the same conditions. The table also shows a bottom, middle and a top sample, representing the section of the sample that was analyzed (bottom being the first part to solidify and top being the last).

Table 7: Carbon content of gray iron samples before directional solidification

Sample	Carbon %
GI Base	4.5
GI #1	3.8
GI #2	3.3
GI #3	3.6
GI #4	3.5

Table 8: Carbon content of directionally solidified gray iron samples at 0.5µm/s

Sample	Section	Carbon %
GI #2	Bottom	2.7
	Middle	3.1
	Top	3.7
GI #3	Bottom	2.7
	Middle (I)	3.2
	Middle (II)	3.4
	Top	3.7

From Table 8 it is visible that as the sample is being solidified the carbon content is higher at the top of the sample. Since the graphite is less dense than the iron, if a piece of graphite solidifies ahead of the solid/liquid interface, it will float to the top of the sample. This suggests that the distance of solidification will have an effect on the carbon percentage of the sample directionally solidified and requires further investigation, since the graphite spacing is likely to be influenced as well.

4. FUTURE WORK

4.1. Additional experimental work

For future projects, thermal undercooling experiments can be performed for determination of the solid/liquid interface temperature. With this information it is possible to determine if there is an effect on the composition of gray iron after directional solidification. Experiments with an increased separation between thermocouples can be included to the developed thermocouples setup to prevent the temperature changes being recorded at the same time. Also the thermocouple setup can be improved by insulating both thermocouples individually with alumina crucibles in order to prevent them from recording any inconvenient thermal data. Furthermore, more directional solidification experiments should be done on the gray iron samples at various velocities of solidification. This will aid in understanding how and what properties will be affected in the material.

For this project, spacing is the parameter that is being studied; however, there are other parameters that can be taken into account for the same type of changes that were made in this study. A study of the mechanical properties, for example, can be done on the

selected directionally solidified samples and compared to regular gray cast iron to determine the difference in mechanical properties.

4.2. Automated MATLAB Code

The analysis presented in the previous sections was done on five samples with different compositions for one directional solidification velocity of 5 μm/s. The purpose of this research is to validate the developed MATLAB automated stereology code to be applicable for any type of spacing measurements. The purpose was achieved with the gray iron samples used for this study. The results show that the measurements that were taken from the automated process accurately output the spacing measurements.

The next step in the improvement of the code is to be able to lower standard deviations in the automated process for all the images that are analyzed. This can be attained by concentrating on the sections of the image that have the closest spacing and improving the code to concentrate on these measurements. Moreover, the automated code can be improved to output minimum and maximum spacing measurements. With the data then a clear range of spacing measurements can be determined. This can be achieved by taking 5% and 95% values from the spacing distribution curve. Also another improvement would be to enhance the code to limit the dimensions of the picture that is selected by the user for calculation to the crossings. This can be achieved by having the code precalculate the maximum crossings section of the image and recommend to the user the maximum number of crossings that can be used for the image to output accurate values.

Additionally, the code can be enhanced to output more accurate values of spacing by improving the pixels that are being scanned by the program. Since there are a lot of

pixels close together where no flake graphite is present, when the code is calculating number of crossings then for this cluster of pixels ends up having the same values of line length. These will then affect the final average value, since it will have a lot more values of the same line length, where the spacing could not be the most accurate minimum possible. This problem can be fixed by then improving the code so it will focus on the pixels of the image where the flake graphite is present. With this suggestion then there will be less pixels to scan, the code will have more accurate values, less deviation and ultimately the time the code takes to process the image will be reduced. Moreover, a more precise average measurement of spacing can be output by the code. The way that it can be achieved is by having the code save all the spacing measurements that are being recorded for an image and once all the images have been processed then the code would calculate an average and standard deviation of all the picked images.

Lastly, more stereology measurements can also be calculated and compared to the manual stereology values in order to have a more objective and time efficient way to characterize a material. The current MATLAB code uses some of the stereology equations that are currently being used in manual stereology. Writing some lines that would output these values in the excel spreadsheet created and compared them to the actual stereology values and determine if the code can also be used for other stereology measurements accurately.

5. CONCLUSIONS

Graphite spacing in gray iron was measured, showing a dependence on both velocity and composition. By adding silicon and manganese, it was found that the spacing measurements slightly decrease; while increasing the velocity of the process will

force the spacing to lose directionality and reduce flake thickness present. Transverse spacing measurements and the carbon percentage versus distance of solidification analysis proved that graphite spacing and the carbon percentage vary with solidification distance.

A comparative analysis between manual and automated stereology spacing measurements were done on gray iron samples with different compositions. From the results it was concluded that the automated process is a more objective and less time consuming way to determine accurate spacing measurements. Even though some of the standard deviations of the samples were higher for the automated process, error difference percentages showed that acceptable range of values were given by the automated process with the parameters proposed.

6. REFERENCES

[1] Degarmo, E., Black, J. T., & Ronald, A. (2003). Materials and Processes in Manufacturing. Wiley.

[2] *Fe-C Phase Diagram-The Basis of the Heat Treatment of Steel*. (2014, December 3). Retrieved from http://www.mrl.ucsb.edu/~edkramer/LectureVGsMat100B/99Lecture14VGs/FeCPhaseDiagramVG.html

[3] Rudnev, V; *Handbook of Induction Heating*, CRC Press, 53.

[4] Piwowarsky, E.; *Hochwertiges Gusseisen*, 2nd Ed.; Springer-Verlag, 1958

[5] Glicksman, M. A.; *Principles of Solidification: An Intoduction to Modern Casting and Crystal Growth Concepts*, Springer, Chapter 15.

[6] Kurz, W.; Fisher, D.J. (1998) *Fundamentals of Solidification.* Trans Tech Publications.

[7] Jones, H., & Kurz, W. (1980). Growth Temperatures and the Limits of Coupled Growth in Unidirectional Solidification of Fe-C Eutectic Alloys. *Metallurgical Transactions A*, 1265-1273.

[8] P. Magnin, W. K. (1988). Competitive Growth of Stable and Metastable Fe-C-X: Part 1. Experiments. *Metallurgical Transactions A*, 1955-1963.

[9] K. D. Lakeland, *BCIRA Journal*, 12 (1964), 634-650.

[10] Jackson, K., & Hunt, J. (1966). *Trans. AIME*, 1129-42.

[11] Bührig, A., & Santos, D. d. (2008). Solidification of Eutectic Alloys-Cast Iron*. *ASM Handbook Volume 15: Casting*, 317-329.

[12] Kagawa, A., & Okamoto, T. (1980). Partition of Silicon during Eutectic Solidification of Iron-Carbon-Silicon Alloy. *Metal Science*, 519-524.

[13] Hendrix, J. C., Curreri, P. A., & Stefanescu, D. M. (1984). Directional Solidification of Flake and Spheroidal Graphite Cast Iron in Low and Normal Gravity Environment. *AFS Transactions*, 435-458.

[14] Stefanescu, D. M., Curreri, P. A., & Fiske, M. R. (1986). Microstructural Variations Induced by Gravity Level during Directional Solidification of Near-Eutectic Iron Carbon Type Alloys. *Metallurgical Transactions A*, 1121-1130.

[15] P. Magnin, W. K. (1988). Competitive Growth of Stable and Metastable Fe-C-X Eutectics: Part II. Mechanisms. *Metallurgical Transactions A*, 1965-1971.

[16] Magnin, P. (1985). *Solidification Competitive Stable/Metastable Des Alliages Fe-C-X Eutectiques*. Ecole Polytechnique Federale de Lausanne; Lausanne, Switzerland.

[17] D.K. Barnerjee, D. M. Stefanescu (1991). Structural Transitions and Solidification Kinetics of SG Cast Iron During Directional Solidification Experiments. *Transactions of the American Foundrymen's Society,* 747-759

[18] L. Nastac (1998). Analytical Modeling of Solute Redistribution During the Initial Unsteady Unidirectional Solidification of Binary Dilute Alloys: Comparison Experiments. *Scripta Materialia,* 985-989.

[19] Guzik, E., & Kopycínski, D. (2006). Modeling Structure Parameters of Irregular Eutectic Growth: Modification of Magnin-Kurz Theory. *Metallurgical and Materials Transactions A*, 3057-3067.

[20] W. Monroe, UAB Casting Group Internal Report, Number: UAB-MTG-15-3101273-80.

[21] Catalina, A.V.; Voorhees, P.W.; Huff, R.K.; Genau, A.L. A model for eutectic growth in multicomponent alloys. *Proc. Advances in the Science and Engineering of Casting Solidification,* TMS 2015.

[22] Gegner, J., & al., e. (2012). Alloy Dependence of the Diffusion Coefficient of Carbon in Austenite and Analysis of Carburization Profiles in Case Hardening of Steels. 261-287.

[23] Minkoff, I. (1983). *The Physical Metallurgy of Cast Iron.* John Wiley and Sons.

[24] MATLAB 8.4, The MathWorks, Inc., Natick, MA, 2014.

[25] Rivera E A, Christiansen T, Genau A, and Catalina A V 2015 *Proc. Advances in the Science and Engineering of Casting Solidification*, TMS 2015.